



AD-A286 556



Technical Report REMR-HY-12
November 1994

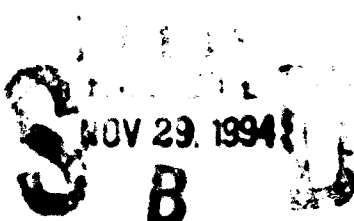
(1)

US Army Corps
of Engineers
Waterways Experiment
Station

Repair, Evaluation, Maintenance, and Rehabilitation Research Program

HIVEL2D: A Two-Dimensional Flow Model for High-Velocity Channels

by R. L. Stockstill, R. C. Berger



Approved For Public Release: Distribution Is Unlimited

94 1128 020

94-36238



Prepared for Headquarters, U.S. Army Corps of Engineers



The following two letters used as part of the number designating technical reports of research published under the Repair, Evaluation, Maintenance, and Rehabilitation (REMR) Research Program identify the problem area under which the report was prepared:

<u>Problem Area</u>		<u>Problem Area</u>	
CS	Concrete and Steel Structures	EM	Electrical and Mechanical
GT	Geotechnical	EI	Environmental Impacts
HY	Hydraulics	OM	Operations Management
CO	Coastal		

The contents of this report are not to be used for advertising, publication, or promotional purposes. Citation of trade names does not constitute an official endorsement or approval of the use of such commercial products.



PRINTED ON RECYCLED PAPER

**Repair, Evaluation, Maintenance, and
Rehabilitation Research Program**

**Technical Report REMR-HY-12
November 1994**

HIVEL2D: A Two-Dimensional Flow Model for High-Velocity Channels

by R. L. Stockstill, R. C. Berger

**U.S. Army Corps of Engineers
Waterways Experiment Station
3909 Halls Ferry Road
Vicksburg, MS 39180-6199**

Final report

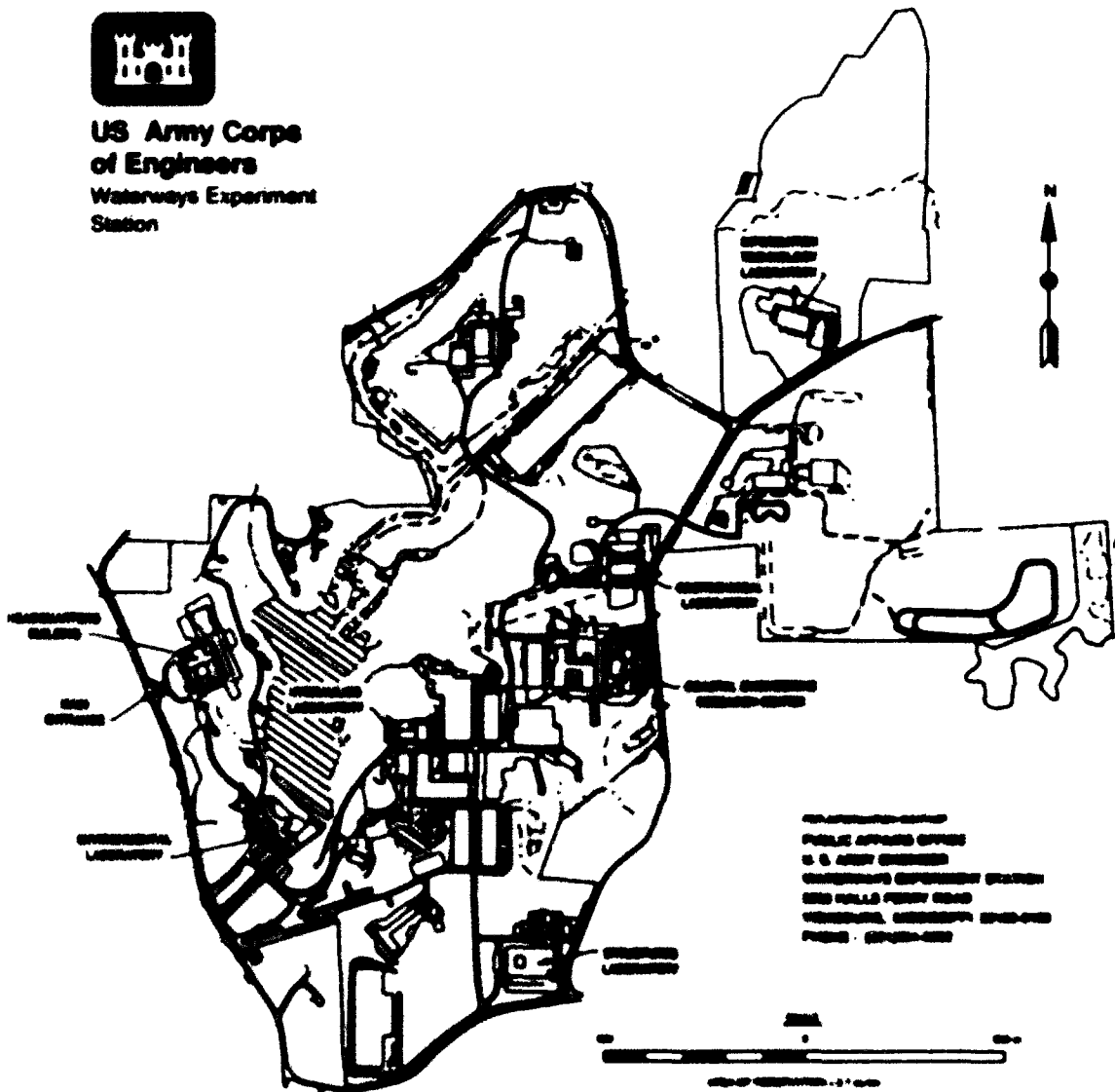
Approved for public release; distribution is unlimited

**Prepared for U.S. Army Corps of Engineers
Washington, DC 20314-1000**

Under Civil Works Research Work Unit 32657



US Army Corps
of Engineers
Waterways Experiment
Station



Waterways Experiment Station Cataloging-In-Publication Data

Stockstill, Richard L.

HIVEL2D : a two-dimensional flow model for high-velocity channels / by R.L. Stockstill,
R.C. Berger ; prepared for U.S. Army Corps of Engineers.

53 p. : ill. ; 28 cm. — (Technical report ; REMR-HY-12)
Includes bibliographic references.

1. Streamflow — Mathematical models. 2. Hydraulic jump — Models. 3. Hydrodynamics — Data processing. 4. River channels. I. Berger, Rutherford C. II. United States. Army. Corps of Engineers. III. U.S. Army Engineer Waterways Experiment Station. IV. Repair, Evaluation, Maintenance, and Rehabilitation Research Program . V. Title. VI. Title: A two-dimensional flow model for high-velocity channels. VII. Series: Technical report (U.S. Army Engineer Waterways Experiment Station) ; REMR-HY-12.

TA7 W34 no.REMR-HY-12

Contents

Preface	iv
Conversion Factors, Non-SI to SI Units of Measurement	v
1—Introduction	1
Background	1
Purpose and Scope	1
2—Description of Model	3
Assumptions	3
Discretization	5
Boundary Conditions	5
3—Test Cases	6
Channel Contraction	6
Hydraulic Jump	7
Supercritical Confluence	8
Bridge Pier	9
Dam Break Problem	10
Roll Waves	12
4—Discussion and Conclusions	13
References	14
Figures 1-26	
Appendix A: Governing Equations	A1
Appendix B: Finite Element Formulation	B1
Petrov-Galerkin Test Function	B5
Shock Capturing	B7
Temporal Derivatives	B8
Solution of the Nonlinear Equations	B9

Preface

The study reported herein was authorized by Headquarters, U.S. Army Corps of Engineers (HQUSACE), as part of the Hydraulics Problem Area of the Repair, Evaluation, Maintenance, and Rehabilitation (REMR) Research Program. The work was performed under Civil Works Research Work Unit 32657, "Model for Evaluation and Maintenance of High-Velocity Channels." The REMR Technical Monitor was Mr. Dave Wingerd (CWCW-EH).

Mr. William N. Rushing (CERD-C) was the REMR Coordinator at the Directorate of Research and Development, HQUSACE. Mr. James E. Crews (CECW-O) and Dr. Tony C. Liu (CWCW-BG) served as the REMR Overview Committee. The REMR Program Manager was Mr. William F. McCleese, U.S. Army Engineer Waterways Experiment Station (WES). Mr. Glenn A. Pickering, Chief, Hydraulic Structures Division (HSD), Hydraulics Laboratory (HL), WES, was the Problem Area Leader. Dr. R. C. Berger, Estuaries Division (ED), HL, and Mr. Richard L. Stockstill, HSD, were Principal Investigators.

This work was conducted by Dr. Berger and Mr. Stockstill under the direct supervision of Mr. Pickering and under the general supervision of Messrs. Frank A. Herrmann, Jr., Director, HL; Richard A. Sager, Assistant Director, HL; William H. McAnally, Jr., Chief, ED; and John P. George, Chief, Locks and Canals Branch, HSD, HL. Mr. Mike W. Orr, HSD, prepared the illustrations.

At the time of publication of this report, Director of WES was Dr. Robert W. Whalin. Commander was COL Bruce K. Howard, EN.

The contents of this report are not to be used for advertising, publication, or promotional purposes. Citation of trade names does not constitute an official endorsement or approval of the use of such commercial products.

Conversion Factors, Non-SI to SI Units of Measurement

Non-SI units of measurement used in this report can be converted to SI units as follows:

Multiply	By	To Obtain
cubic foot	0.02831685	cubic meters
degrees (angle)	0.01745329	radians
foot	0.3048	meters
square foot	0.09290304	square meters

Accession Per

STIS GRAAI	<input checked="" type="checkbox"/>
DTIC TAB	<input type="checkbox"/>
Unannounced	<input type="checkbox"/>
Justification	
By _____	
Distribution/ _____	
Availability Codes	
Dist	Avail and/or Special
R-1	

1 Introduction

Background

The hydraulic performance of a high-velocity channel depends on maintaining a supercritical flow regime over specified portions of its length. Predicting the potential location of shocks, such as oblique standing waves and hydraulic jumps, and determining the superelevation of the water surface in channel bends are necessary to evaluate and maintain the required wall heights. Typically empirical equations or physical hydraulic models have been used to make these evaluations.

Physical models were used in the original study of many existing flood-control channels, but urbanization within their drainage basins has resulted in discharges greater than those for which the channel was originally designed. Obstacles, such as debris or bridge piers, may cause the flow to jump to a subcritical state, thus resulting in flood damage. Therefore, an inexpensive and a readily available means for evaluating these channels is needed. A numerical model is a logical approach.

A numerical flow model, HVEL2D, has been developed as a tool to evaluate high-velocity channels which are man-made concrete lined channels with hydraulically steep slopes. The successful design of high-velocity channels depends on accurate predictions of the flow depths. HVEL2D is a depth-averaged, two-dimensional (2-D) flow model designed specifically for flow fields that contain supercritical and subcritical regimes as well as the transitions between the regimes. The model does not include Coriolis or wind effects, and sediment transport is not addressed since these phenomena are not applicable to concrete lined channels.

Purpose and Scope

The purpose of this report is to describe the numerical flow model, HVEL2D, and to illustrate typical high-velocity flow fields that the model is capable of simulating. These model verifications consist of comparing results computed using HVEL2D with laboratory data. Model limitations are also discussed. It is important that HVEL2D users understand which flow

situations are suited to simulation using HIVEL2D and which are not.

A user's manual will be the second report published for this work unit. The user's manual will discuss such topics as grid generation (FastTABS), hardware requirements (personal computers (PC's) and/or workstations), time involved in grid generation and simulation runs, and guidance relative to grid layout and parameter choice.

2 Description of Model

The model is designed to simulate flow typical in high-velocity channels. The model is a finite element description of the 2-D shallow-water equations in conservative form. Specifically, the model is designed to provide the water surface in and around boundary transitions, bridge piers, confluences, bends, and other geometric features common in high-velocity channels. HIVEL2D is applicable to sub- and supercritical flow and the transitions between these regimes.

The system of nonlinear equations are solved using the Newton-Raphson iterative method. The Newton-Raphson method was selected for this model because the nonlinear terms in high-velocity channel flow fields are quite significant.

Stresses are modeled using the Manning's formulation for boundary drag and the Boussinesq relation for Reynolds stresses. Eddy viscosities are approximated using an empirical relation based on Manning's coefficient and local flow variables.

Assumptions

HIVEL2D solves the depth-averaged unsteady shallow-water equations implicitly using finite elements. The governing equations are presented in detail in Appendix A.

An important (and standard) assumption made in the derivation of the governing equations is that vertical accelerations are negligible when compared to the horizontal accelerations and acceleration due to gravity. This assumes that the pressure distribution is hydrostatic. The hydrostatic pressure assumption is generally applicable to high-velocity channels. However, care must be taken in applying the model to flow situations where the wavelength is not long relative to the depth. All hydrostatic models overestimate the speed of short wavelengths.

To understand why short wavelengths travel more slowly than longer wavelengths, consider the vertical momentum equation:

$$\frac{1}{\rho} \frac{\partial P}{\partial z} = - \left(\frac{dw}{dt} \right) - g \quad (1)$$

where

ρ = fluid density

P = pressure

z = vertical Cartesian coordinate

w = the z -direction component of velocity

t = time

g = acceleration due to gravity

Near the crest of a wave, or anywhere that the water surface is convex, the fluid element riding near the surface has a negative vertical acceleration, i.e., $dw/dt < 0$. Therefore, the vertical acceleration acts opposite to gravity and pressure is reduced. Conversely, near the trough where the water surface is concave, the near-surface fluid element has a positive acceleration, and so acts to enhance the pressure. The net effect is that the surface curvature reduces the pressure gradients and the wave will travel more slowly. The shorter the wavelength, the slower it will tend to propagate. For long wavelengths this impact is negligible.

Another consequence of the hydrostatic assumption is that the shallow-water equations can provide no information about the length of a jump, i.e., distance from the leading to the trailing edge of a hydraulic jump. The shallow-water equations contain no vertical velocity or acceleration; therefore, any energy that should be captured in vertical motion is lost. The shallow-water equations must simulate the jump as a discontinuity and all vertical energy is immediately dissipated. This is unlike the real system in which an undular jump may form that dissipates this vertical motion over a long distance.

Another significant assumption is that the bed slope is geometrically mild so that $\sin \theta = \tan \theta = \theta$, where θ is the channel slope. This geometrically mild slope assumption is distinguished from a hydraulically mild slope that conveys flow as subcritical (i.e., the shallow water equations assume that the slope is geometrically mild, although it may be hydraulically steep). This is a reasonable assumption in most high-velocity channel applications where the slope is less than 0.02. However, when application is made to a long channel reach having a favorable slope in excess of say 0.05, the mild slope assumption will tend to overestimate the flow speed and underestimate the flow depth.

Discretization

Discrete values of the unknown variables are solved using a Petrov-Galerkin finite element formulation of the governing equations. Details of the finite element formulation are presented in Appendix B. The model is quite stable as a result of the particular Petrov-Galerkin test function employed, which is weighted upstream along characteristic lines. The finite element model reproduces triangular and quadrilateral bilinear elements and can be easily modified to capture complex geometries.

HIVEL2D solves the finite element equations using the weak formulation. The weak formulation facilitates the specification of natural boundary conditions and allows accurate shock capturing, which is essential in modeling supercritical flow.

Temporal derivatives are solved implicitly using a finite difference discretization. The temporal derivatives can be approximated using either a first-order ($\alpha = 1.0$) or second-order ($\alpha = 1.5$) backward difference. A first-order difference is used for the spin-up to a steady flow solution, whereas a second-order difference is more appropriate for unsteady flow simulation.

Boundary Conditions

Inflow and outflow boundary conditions can be specified as supercritical or subcritical. Supercritical inflow boundaries require the specification of the three degrees of freedom (i.e., the x- and y-components of unit discharge and the depth or the x- and y-components of velocity and the depth). Subcritical inflow boundaries require that only two specific degrees of freedom be given (i.e., the x- and y-components of unit discharge or the x- and y-components of velocity). Boundary conditions at supercritical outflow boundaries should not be specified. Subcritical outflow boundaries require the specification of tailwater elevation (i.e., depth plus bed elevation).

Sidewall boundary conditions are enforced using the weak statement. The boundary conditions enforced are that the mass and momentum flux through the sidewalls are zero. Sidewalls also enforce a partial slip condition.

3 Test Cases

Numerous test cases are presented to illustrate the model's ability to simulate high-velocity channel flow fields. More importantly, results of test cases point out flow conditions that are not accurately modeled by HIVEL2D. The model user must understand when the model's governing equations are adequate for the particular problem to be solved and when they are not. It is demonstrated that the numerical scheme accurately solves the depth-averaged 2-D equations. The depth-averaged equations appropriately describe most high-velocity channel flow fields.

Several features commonly found in high-velocity channels are included in the test cases: simulations of channel contractions, expansions, confluences, bends, hydraulic jumps, bridge piers, bores, and roll waves.

Input parameters for each simulation are provided in tabular form: the temporal difference coefficient α ; the Petrov-Galerkin weight coefficient β (for smooth flow) and β_s (for flow near shocks); Manning's coefficient n ; the eddy viscosity ν (for smooth flow) and ν_s (for flow near shocks); and the acceleration due to gravity g . Detailed descriptions of the temporal difference and Petrov-Galerkin weight coefficients are provided in Appendix B. Early tests were conducted using a version of HIVEL2D that used a constant user-specified eddy viscosity for the entire flow field. The current version of HIVEL2D varies the viscosity based on local flow variables. Details of how viscosities are determined are presented in Appendix A.

Channel Contraction

Initially, HIVEL2D was run to simulate supercritical flow in a channel contraction. A laboratory investigation of supercritical flow in channel contractions was reported by Ippen and Dawson (1951) in which depth contours were presented. One particular test documented flow conditions in a straight-wall contraction with an approach Froude number of 4.0. The straight-wall contraction was a 2-ft- (0.61-m-) wide¹ channel, transitioning to

¹ A table of factors for converting non-SI units of measurement to SI units is found on page v.

a 1-ft- (0.30-m-) wide channel at a convergence angle of 6 deg. The grid used for the simulation is provided in Figure 1. The grid consisted of 1661 nodes and 1500 elements. The long approach length of 20 ft was used to ensure uniform flow conditions at the contraction. Figure 2 shows contours of flow depth observed in the laboratory and those computed using HVEL2D for a discharge of 1.44 cfs (0.041 cms) and an upstream Froude number of 4.0. Input parameters used in the numerical simulation are provided in Table 1. A water-surface mesh generated using these HVEL2D results is shown in Figure 3.

The contraction is a geometrically simple case, but the results demonstrate the model's ability to capture the oblique standing waves resulting from changes in the wall boundaries. Oblique standing waves are created as the supercritical velocity encounters the converging sidewalls. These standing waves are reflected from opposing sidewalls for a distance downstream. HVEL2D captures the standing waves and the depth increase as the waves intersect at the channel center line.

Table 1
Input Parameters for the Channel Contraction

Condition	Value
<i>a</i>	1.0
<i>B.B.</i>	0.1, 0.5
<i>n</i>	0.011
<i>v.v.</i>	0.005, 0.005 ft ³ /sec (4.65 × 10 ⁻⁴ m ³ /sec)
<i>g</i>	32.208 ft/sec ² (9.817 m/sec ²)

Hydraulic Jump

Tests were conducted to compare the results from HVEL2D with some of those obtained in the physical model study of Rio Puerto Nuevo Flood-Control Channel (Stockstill and Leech 1990) conducted for the U.S. Army Engineer District, Jacksonville. Three models were constructed and tested for the Puerto Nuevo study. These models were selected for comparisons with HVEL2D calculations simply because the channels' geometric and hydraulic details were at hand and several features common to high-velocity channels were included. Specifically, the Puerto Nuevo study channels contained supercritical confluences, horizontal curves, expansions, and a tailwater-imposed hydraulic jump. To avoid similitude questions, HVEL2D was run at laboratory scale. This resulted in direct comparisons of calculations to observed quantities.

The Margarita Channel was one of the three models tested for the project. The Margarita Channel consisted of two reverse curves separated by a short

tangent, a channel expansion, and tailwater that produced a hydraulic jump upstream of the width transition. Details of the modeled reach of the Margarita Channel are presented in Figure 4. Input parameters used in modeling the Margarita Channel are provided in Table 2, and the finite element grid is shown in Figure 5. Typically when steady-state solutions are sought, a first-order temporal derivative is appropriate and an $\alpha = 1.0$ is used. Because portions of the Margarita Channel exhibited unsteady flow features, an $\alpha = 1.5$ was used resulting in a second-order temporal derivative. The finite element grid consisted of 796 nodes and 651 elements. Figure 6 compares water-surface profiles along the channel walls for a discharge of 1.2 cfs (0.034 cms) with a tailwater depth at the downstream end of the model of 0.601 ft (0.183 m).

Table 2
Input Parameters for the Margarita Channel

Condition	Value
α	1.5
$B.B.$	0.2, 0.5
n	0.010
$v.v.$	0.008, 0.025 ft ² /sec (7.43 × 10 ⁻⁴ , 2.32 × 10 ⁻⁴ m ² /sec)
g	32.208 ft/sec ² (9.817 m/sec ²)

HIVEL2D not only captured the hydraulic jump in the channel, but also reproduced the asymmetric flow patterns downstream of the width transition that were observed in the physical model. The short length of the transition (1 transverse on 4 longitudinal) in conjunction with the asymmetric flow distribution produced by the upstream bend resulted in a large eddy in the downstream channel that produced flow concentrations along the left wall. Depth-averaged velocities at three stations are presented in Figures 7-9. Higher velocities (1.9 fps (0.58 mps)) existed along the left wall whereas the flow along the right wall was essentially stagnant as shown by the dark area in Figure 10. The numerical model results shown in Figure 11 show that HIVEL2D accurately predicted the asymmetric flow patterns downstream of the expansion.

Supercritical Confluence

The numerical model was further tested by comparing computed results of the Puerto Nuevo/Guaracanal Channel confluence with those observed in the laboratory study. Geometric details of the supercritical confluence are provided in Figure 12. Table 3 lists the input parameters, and Figure 13 shows the finite element grid, which is composed of 491 nodes and 390 elements. Boundary conditions for these tests were supercritical inflow with 3.6 cfs (0.10 cms) in the main channel and 1.1 cfs (0.03 cms) in the tributary channel

Table 3
Input Parameters for the Supercritical Confluence

a	1.0
B_B	0.1, 0.5
n	0.009
v, v_s	0.006, 0.005 ft ² /sec (4.65 × 10 ⁻⁴ m ² /sec)
g	32.208 ft/sec ² (9.817 m/sec ²)

and supercritical outflow. Figures 14 and 15 show that the HIVEL2D captured the overall features of the diamond-shaped standing wave pattern resulting from the confluence geometry. The water surface contours shown in Figure 15 illustrate the model's ability to simulate superelevation in the water surface within the tributary channel bend. Water-surface profiles along the flume walls obtained using HIVEL2D and those observed in the laboratory are presented in Figure 16. In most supercritical channels the water surface oscillates in time even under steady boundary conditions. The recorded laboratory results are the maximum water-surface elevations observed, whereas the numerical model represents average water-surface elevations. HIVEL2D adequately simulated the initial shock wave crest, but the location of each subsequent wave crest was increasingly in error. This difference is due to the shallow-water assumption used in the 2-D numerical model. The shallow-water assumption results in all waves traveling with the celerity of a long wave, whereas three-dimensional flow is actually composed of many wave speeds, the maximum of which is the long-wave celerity. The larger wave speed means that the standing wave angles will be greater than the three-dimensional waves. Generally, this shallow-water equation limitation should be of little consequence since channel wall heights are set to contain the maximum water-surface elevation plus freeboard.

Bridge Pier

A hypothetical bridge pier was tested to demonstrate HIVEL2D's ability to simulate a Class B bridge in which the piers choke the flow such that the approaching flow is subcritical even though the channel slope is hydraulically steep. The channel was 100 ft (30.5 m) wide by 1,000 (305 m) ft long. Two piers were used to choke the flow. Each pier was 20 ft (6.1 m) wide by 100 ft (30.5 m) long with a square nose and tail. The finite element grid for the bridge pier problem was composed of 993 nodes and 900 elements (Figure 17).

Water-surface meshes calculated using HIVEL2D are shown in Figures 18 and 19. Table 4 lists input parameters for this simulation. The flow approaching the piers was subcritical and accelerated around the piers to supercritical. The imposed tailwater resulted in a hydraulic jump immediately downstream of the piers. The hypothetical problem demonstrates HIVEL2D's

Table 4
Input Parameters for the Bridge Pier Problem

Condition	Value
a	1.0
β, β_s	0.2, 0.5
n	0.020
v, v_s	10.0, 10.0 ft ³ /sec (0.93 m ³ /sec)
g	32.208 ft/sec ²

ability to model subcritical flow, the transition to supercritical flow, and also the transition to subcritical flow via the hydraulic jump.

Dam Break Problem

Unsteady flow simulations were conducted to test HIVEL2D's discretization to the temporal derivatives of the governing equations. Results were compared to hydraulic flume results reported in Bell, Elliot, and Chaudhry (1992). A plan view of the flume facility is shown in Figure 20. The flume, constructed of Plexiglas, simulated a dam break through a horseshoe bend. Because this was a 2-D problem and model results were being compared to hydraulic flume results, the limitations of the shallow-water equations themselves needed to be considered. Initially, the reservoir had an elevation of 0.1898 m relative to the channel bed; the channel itself was at a depth (and elevation) of 0.0762 m. The velocity was zero and then the dam was removed. The surge location and height were recorded at several stations and compared to the model at three of these, at stations 4, 6, and 8. Station 4 was 6.00 m from the dam along the channel center line in the center of the bend, Station 6 was 7.62 m from the dam near the conclusion of the bend, and Station 8 was 9.97 m from the dam in a straight reach. The model-specified parameters are shown in Table 5.

Table 5
Test Conditions For The Dam Break Case

Condition	Value
a	1.0, 1.5
β, β_s	0.25, 0.50
n	0.009
v, v_s	0.001, 0.01 m ³ /sec
g	9.802 m/sec ²
Δt	0.05 sec

The numerical grid (Figure 21) contains 698 elements and 811 nodes. This grid was reached by increasing the resolution until the results no longer changed. The most critical reach was in the region of the contraction near the dam breach. The basic element length in the channel was 0.1 m with five elements across the channel width. For the smooth channel case, Bell, Elliot, and Chaudhry (1992) used a one-dimensional calculation to estimate the Manning's n to be 0.016, but experience at the U.S. Army Engineer Waterways Experiment Station suggests that this value should actually be 0.009 (Brater and King 1976).

The test results for stations 4, 6, and 8 are shown in Figures 22-24. Here the time-history of the water elevation is shown for the inside and outside of the channel for both the numerical model (at α of 1.0 and 1.5) and the flume. The inside wall is designated by squares and the outside by diamonds. Of particular importance is the arrival time of the shock front. At station 4 the numerical prediction of arrival time using α of 1.0 was about 3.4 sec, which appears to be about 0.05 sec sooner than for the flume. This is roughly 1-2 percent fast. For α of 1.5 the time of arrival was 3.55 sec, which is about 0.1 sec late (3 percent). At station 6 both flume and numerical model arrival times for α of 1.0 were about 4.3 sec, and for station 8 the numerical model was 5.6 sec and the flume was 5.65 to 5.8 sec. With α set at 1.5, the time of arrival was late by about 0.2 and 0.15 sec at stations 6 and 8, respectively. The flume at stations 6 and 8 had an earlier arrival time for the outer wave compared to the inner wave. The numerical model did not show this. In comparing the water elevations between the flume and the numerical model, it is apparent that the flume results show a more rapid rise. The numerical model is smeared somewhat in time, likely as a result of the first-order temporal derivative calculation of α of 1.0. The numerical model with α set at 1.5 shows an overshoot. This is likely a numerical artifact and not based upon physics even though this looks much like the flume results. The surge elevations predicted by the numerical model are fairly close if one notices that the initial elevation of the flume data was supposed to be 0.0762 m and it appears to be recorded as much as 0.015 m higher at some gauges. Since the velocity was initially zero, then all of these readings should have been 0.0762 m and all should be adjusted to match this initial elevation.

With this in mind, stations 4 and 8 match fairly closely between flume and numerical model. Station 4 in the flume would still have a greater difference between outer and inner wave than that predicted by the model. The difference might be a manifestation of a three-dimensional effect that the model cannot mimic. The overall timing and height comparisons are good.

Figure 25 shows the spatial profile of the outer wall water-surface elevation of the numerical model versus distance downstream from center line of the dam. The two conditions are for α of 1.0 and 1.5, i.e., first- and second-order temporal derivative.

The nodes are delineated by the symbols along the lines. The overshoot of the second-order scheme and the damping of the first-order are obvious.

Again, it is probable that the overshoot is a numerical artifact even though this is much like what the flume would show.

Roll Waves

Roll waves are a phenomenon of a high Froude number environment. If the Froude number is greater than 2, it can be shown that disturbances can grow into shocks, which progress downstream faster than the flow. This results in a characteristic sawtooth-shaped water-surface pattern in which the steep face is downstream. The roll wave tests used a modified version of HIVE2D in which a sinusoidal perturbation was input at the upstream boundary of a long straight channel. The water depth results, shown in Figure 26, demonstrate the gradual steepening of the downstream wave face downstream from inflow point. While this is a qualitative comparison, the model does demonstrate the capacity to reproduce this characteristic event.

4 Discussion and Conclusions

This series of tests demonstrates the ability of the model HVEL2D to supply engineering decision makers with a tool to evaluate hydraulic results of structural modifications in supercritical channels.

The code itself is relatively flexible with the one major limitation that the boundary conditions are constant over a simulation. The most significant limitations are therefore imposed by the equations modeled. These are the shallow-water equations employing the mild geometric slope assumption and hydrostatic pressure distribution. The obvious result is that one would not want to use the model to evaluate features with steep slopes. However, the hydrostatic assumption is more subtle. The result of this assumption is that shorter wavelengths will tend to propagate too quickly in the model. This was particularly noted in the supercritical confluence tests. While the water-surface predictions were good over the first reflection or so, they became progressively worse downstream. Another consequence of the hydrostatic assumption is that energy is dissipated too quickly. The result is that energy that should be captured in vertical motion is neglected and undular jumps are instead modeled as strong jumps. Shallow-water models in which vertical motions are assumed negligible cannot predict the length of a hydraulic jump.

References

- Abbott, M. B. (1979). *Computational hydraulics, elements of the theory of free surface flows*. Pitman Advanced Publishing Limited, London.
- Bell, S. W., Elliot, R. C., and Chaudhry, M. H. (1992). "Experimental results of two-dimensional dam-break flows," *Journal of Hydraulic Research* 30(2), 225-252.
- Berger, R. C. (1992). "Free-surface flow over curved surfaces," Ph.D. diss., University of Texas at Austin.
- Berger, R. C. (1993). "A finite element scheme for shock capturing," Technical Report HL-93-12, U.S. Army Engineer Waterways Experiment Station, Vicksburg, MS.
- Berger, R. C., and Winant, E. H. (1991). "One dimensional finite element model for spillway flow." *Hydraulic engineering, Proceedings, 1991 National Conference, ASCE, Nashville, Tennessee, July 29-August 2, 1991*. Richard M. Shane, ed., New York, 388-393.
- Brater, E. F., and King, H. W. (1976). *Handbook of hydraulics*. McGraw-Hill, New York, 7-22.
- Carnahan, B., Luther, H. A., and Wilkes, J. O. (1969). *Applied numerical methods*. Wiley, 319.
- Chapman, R. S. and Kuo, C. Y. (1985). "Application of the two-equation k- ϵ turbulence model to a two-dimensional, steady, free surface flow problem with separation," *International Journal for Numerical Methods in Fluids* 5, 257-268.
- Courant, R., Isaacson, E., and Rees, M. (1952). "On the solution of nonlinear hyperbolic differential equations," *Communication on Pure and Applied Mathematics* 5, 243-255.

- Dendy, J. E. (1974). "Two methods of Galerkin-type achieving optimum L^2 rates of convergence for first-order hyperbolics," *SIAM Journal of Numerical Analysis* 11, 637-653.
- Drolet, J., and Gray, W. G. (1988). "On the well posedness of some wave formulations of the shallow water equations," *Advances in Water Resources* 11, 84-91.
- Gabutti, B. (1983). "On two upwind finite difference schemes for hyperbolic equations in non-conservative form," *Computers and Fluids* 11(3), 207-230.
- Hicks, F. E., and Steffler, P. M. (1992). "Characteristic dissipative Galerkin scheme for open-channel flow," *Journal of Hydraulic Engineering, ASCE*, 118(2), 337-352.
- Hughes, T. J. R., and Brooks, A. N. (1982). "A theoretical framework for Petrov-Galerkin methods with discontinuous weighting functions: Applications to the streamline-upwind procedures." *Finite elements in fluids*. R. H. Gallagher, et al., ed., Wiley, London, 4, 47-65.
- Ippen, A. T., and Dawson, J. H. (1951). "Design of channel contractions." *High-velocity flow in open channels: A symposium. Transactions of the American Society of Civil Engineers* 116, 326-346.
- Katopodes, N. D. (1986). "Explicit computation of discontinuous channel flow," *Journal of Hydraulic Engineering, ASCE*, 112(6), 456-475.
- Praagman, N. (1979). *Numerical solution of the shallow water equations by a finite element method*. EGNER, Den Helder, The Netherlands.
- Moretti, G. (1979). "The λ -scheme," *Computers in Fluids* 7(3), 191-205.
- Rodi, W. (1980). "Turbulence models and their application in hydraulics - a state of the art review," State-of-the Art Paper, International Association for Hydraulic Research, Delft, The Netherlands.
- Steger, J. L., and Warming, R. F. (1981). "Flux vector splitting of the inviscid gas dynamics equations with applications to finite difference methods," *Journal of Computational Physics* 40, 263-293.
- Stockstill, R. L., and Leech, J. R. (1990). "Rio Puerto Nuevo Flood-Control Project, San Juan, Puerto Rico; Hydraulic model investigation," Technical Report HL-90-18, U.S. Army Engineer Waterways Experiment Station, Vicksburg, MS.
- Verboom, G. K., Stelling, G. S., and Officier, M. J. (1982). "Boundary conditions for the shallow water equations," *Engineering applications of computational hydraulics*. M. B. Abbott and J. A. Cunge, eds., vol. 1, Pitman Publishing, Marshfield, MA, 230-262.



Figure 1. Numerical model computational mesh for the channel contraction problem

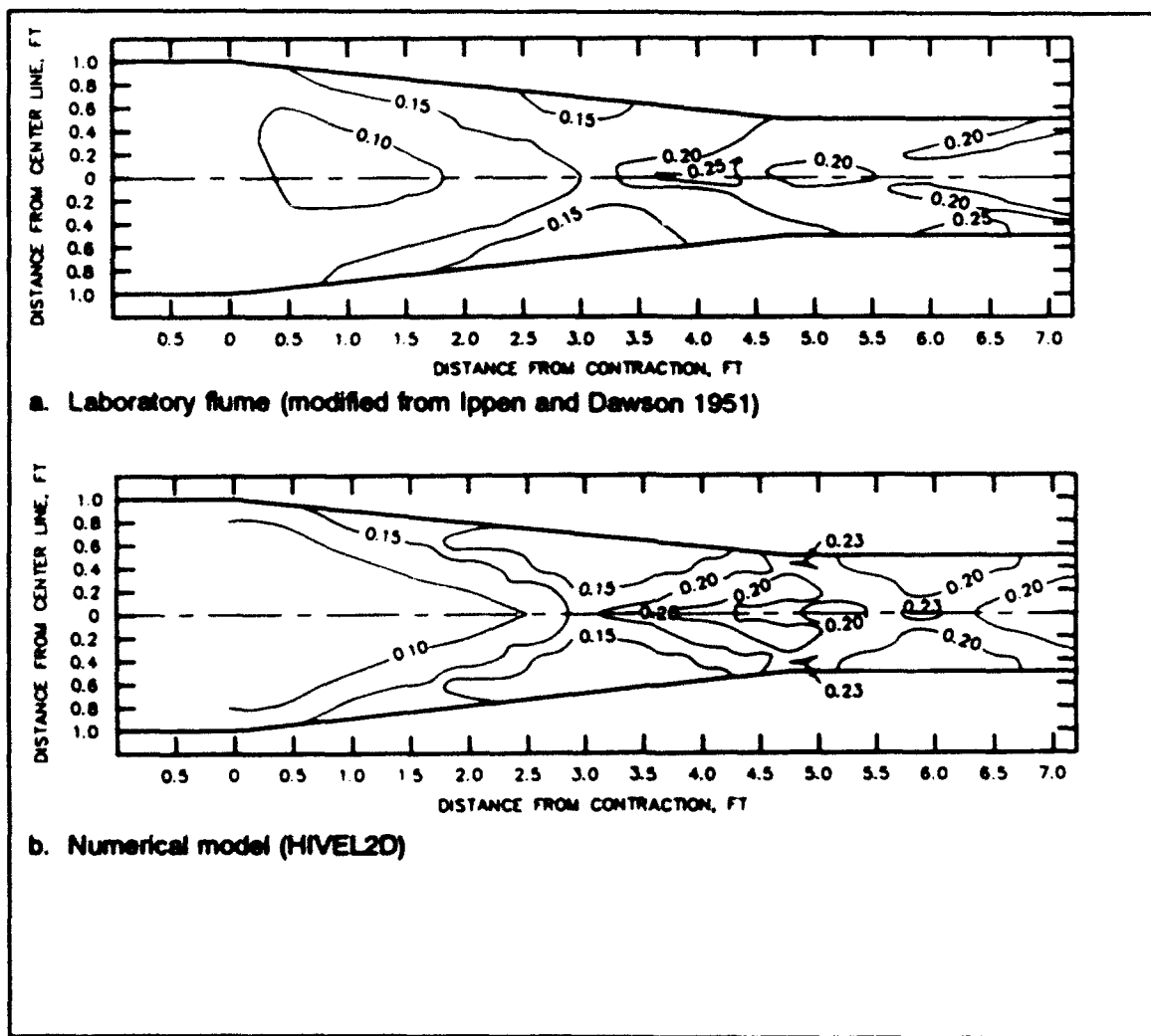


Figure 2. Depth contours of supercritical flow in a contraction

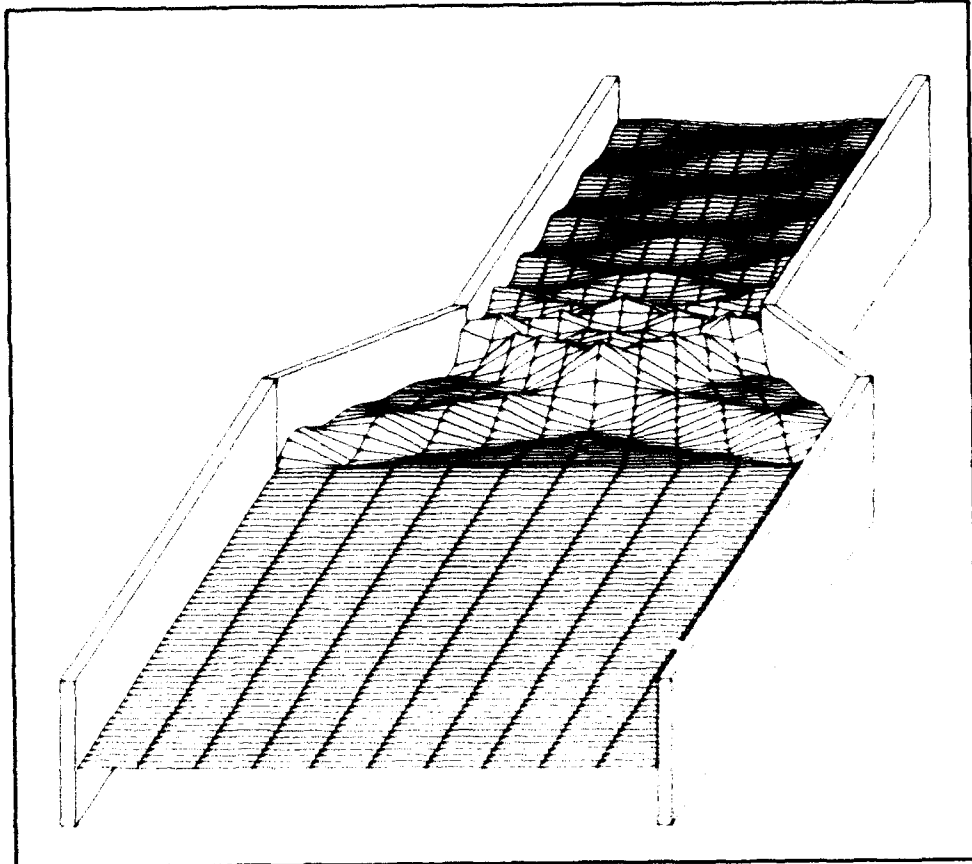


Figure 3. Water-surface mesh of supercritical flow in a contraction

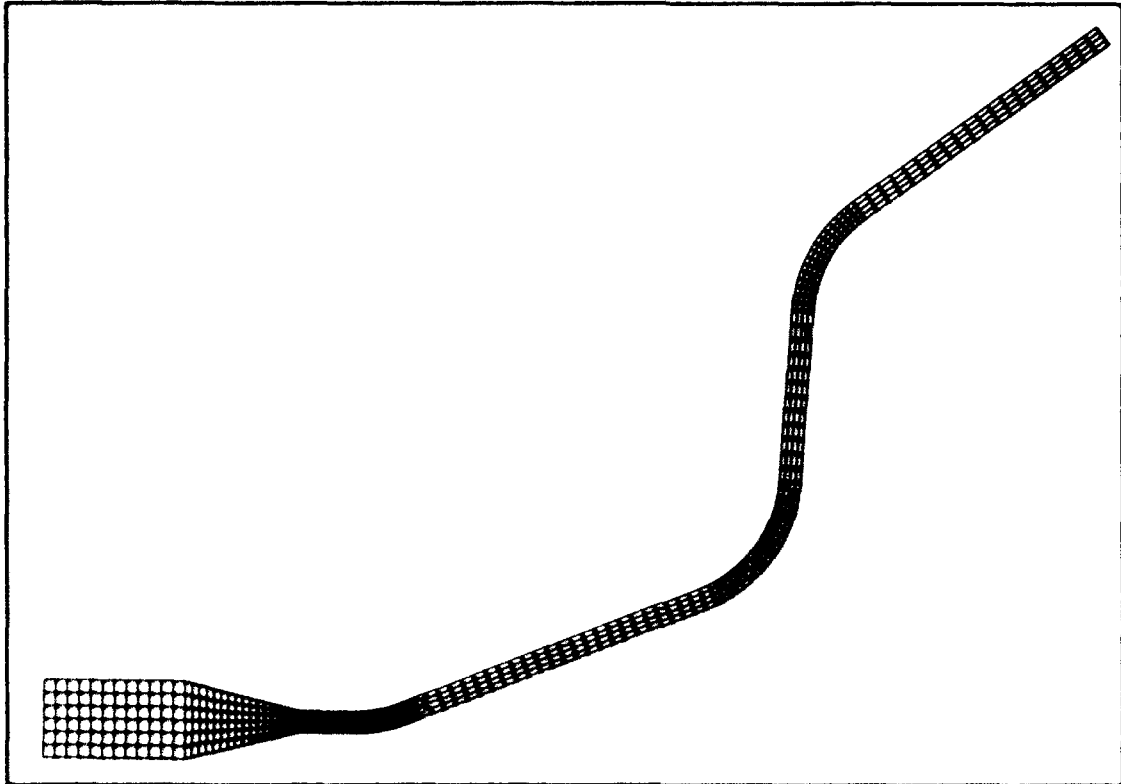


Figure 5. Numerical model computational mesh for the Margarita Channel flume problem

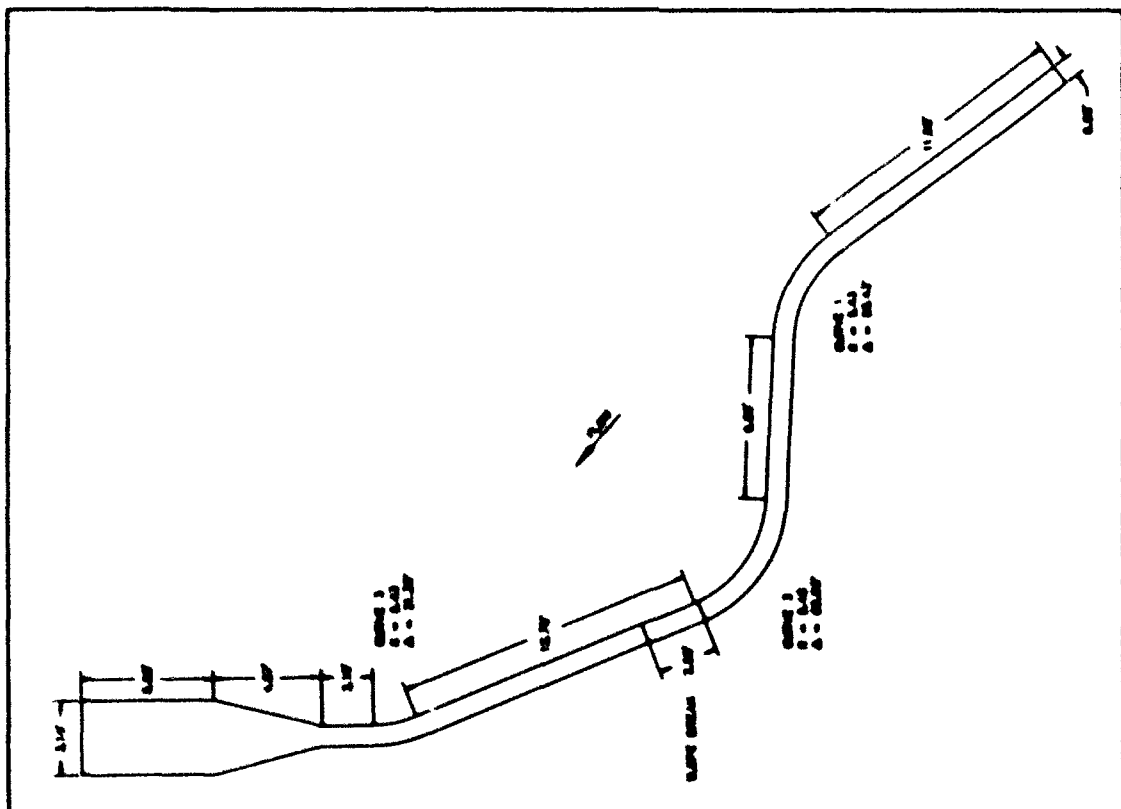


Figure 4. Margarita Channel flume details

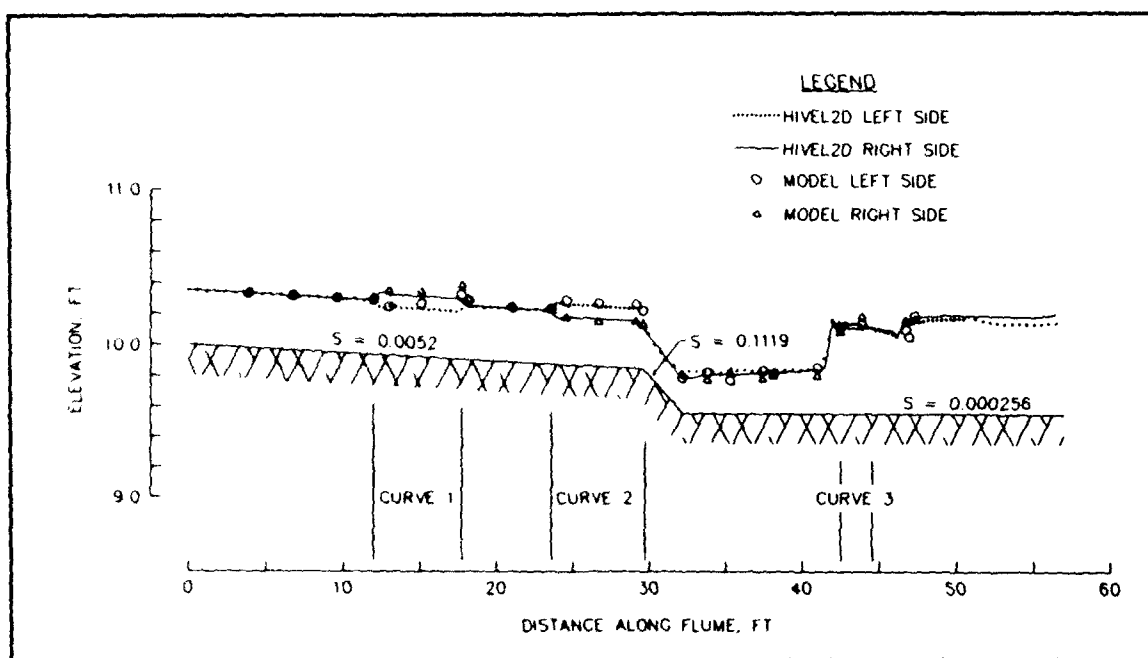


Figure 6. Water-surface profiles of Margarita Channel flume

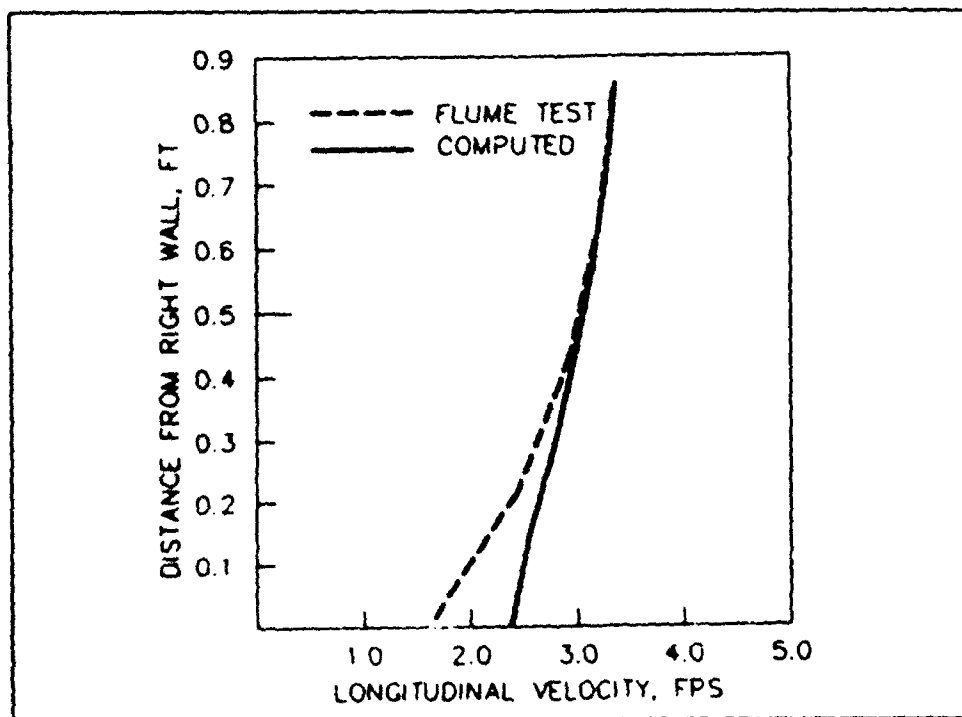


Figure 7. Lateral distributions of longitudinal velocity in Margarita Channel at station 1

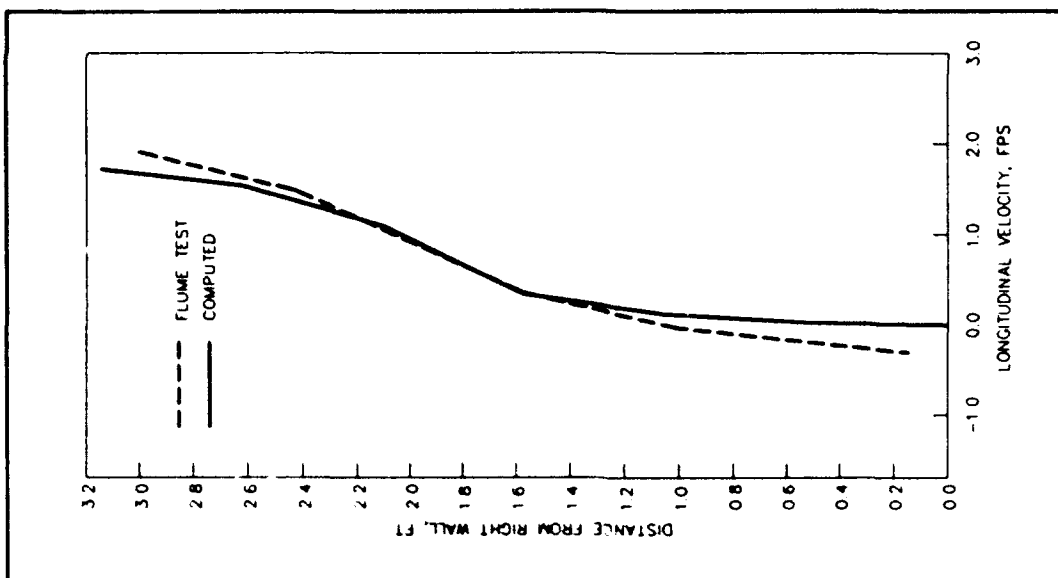


Figure 9. Lateral distributions of longitudinal velocity in Margarita Channel at station 3

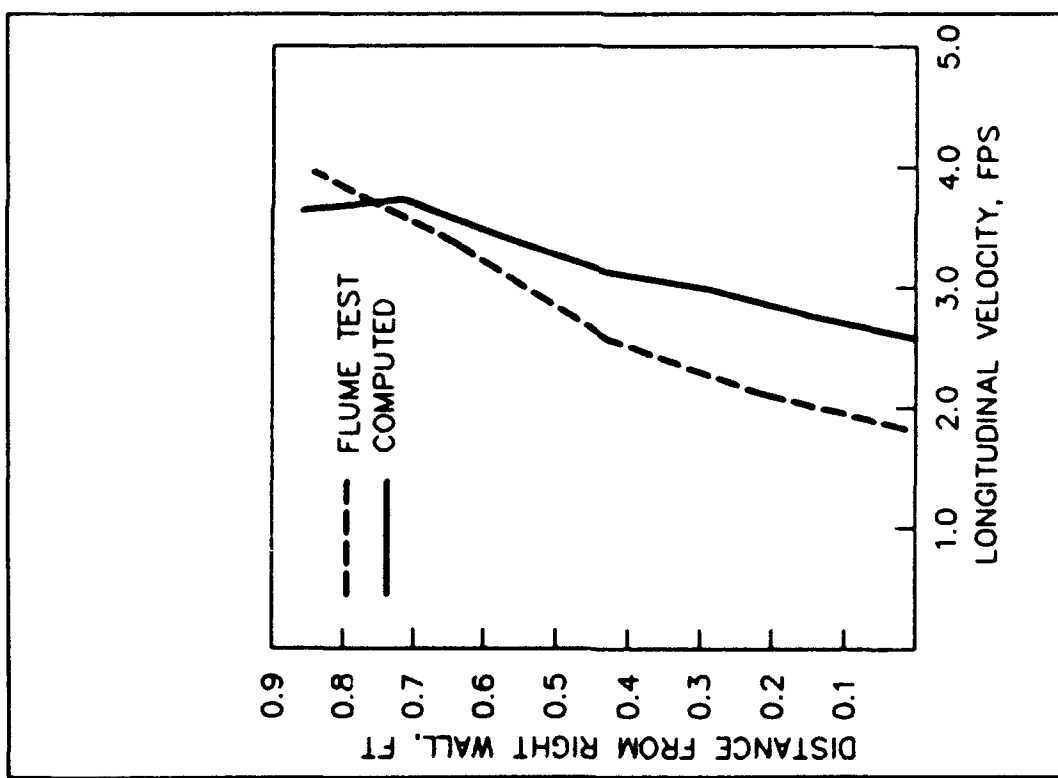


Figure 8. Lateral distributions of longitudinal velocity in Margarita Channel at station 2



Figure 10. Flow conditions in the Margarita Channel physical model

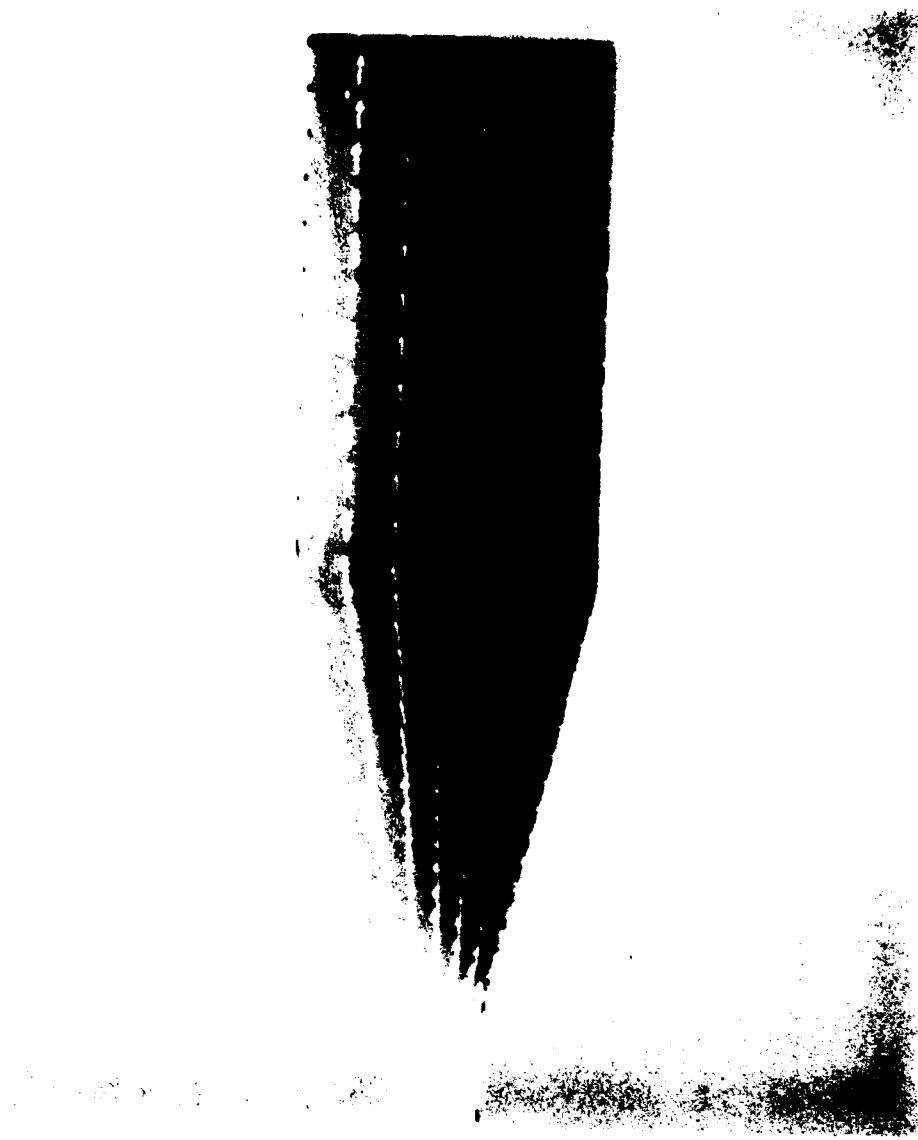


Figure 11. HVEL2D results of Margarita Channel. Velocity contours and vectors (darker contours indicate lower velocities)

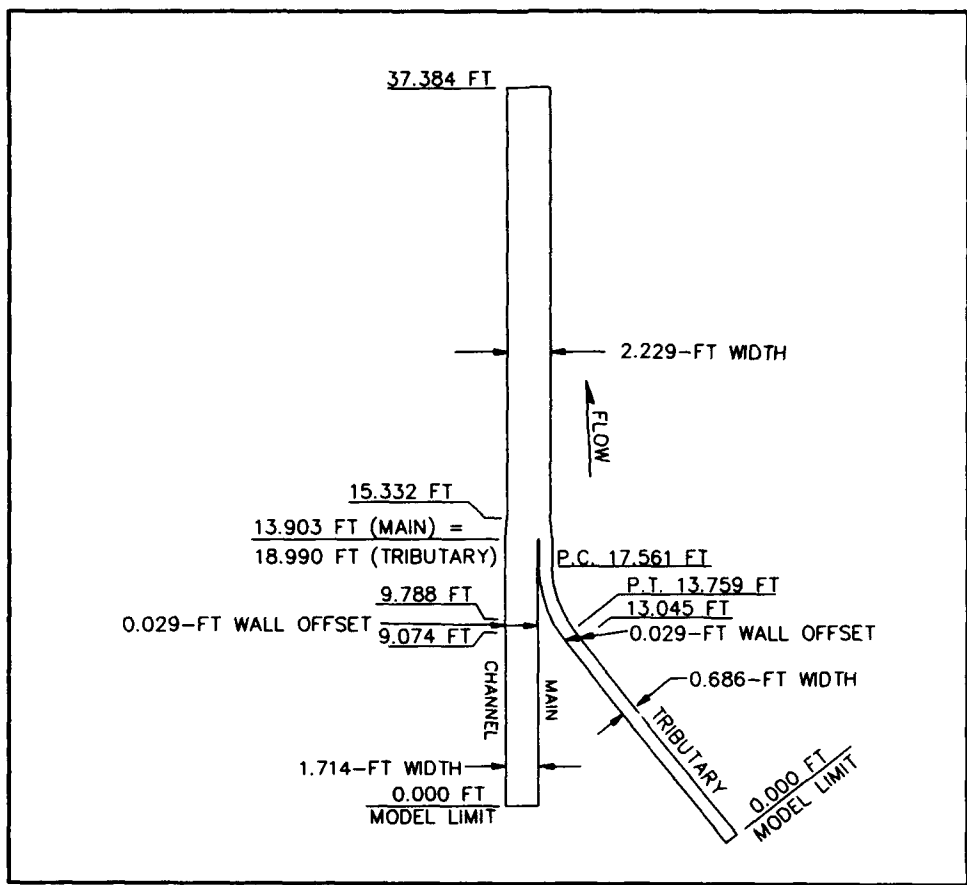


Figure 12. Details of supercritical confluence

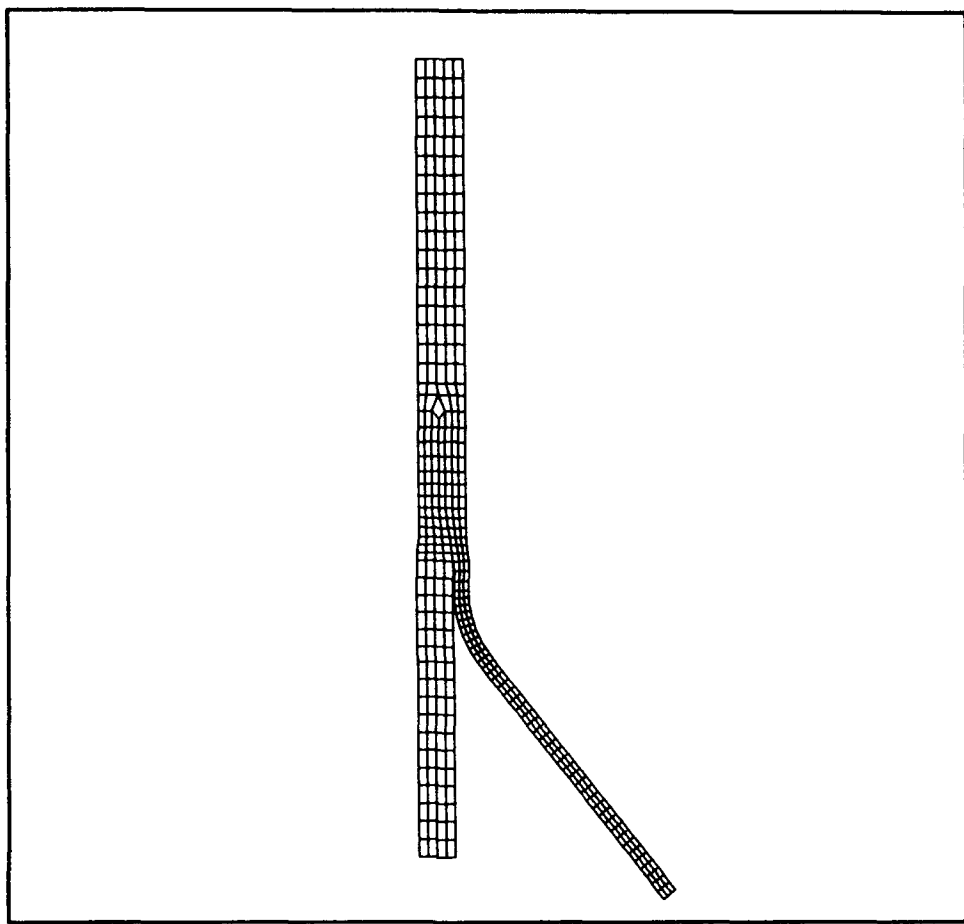


Figure 13. Numerical model computational mesh for the supercritical confluence problem

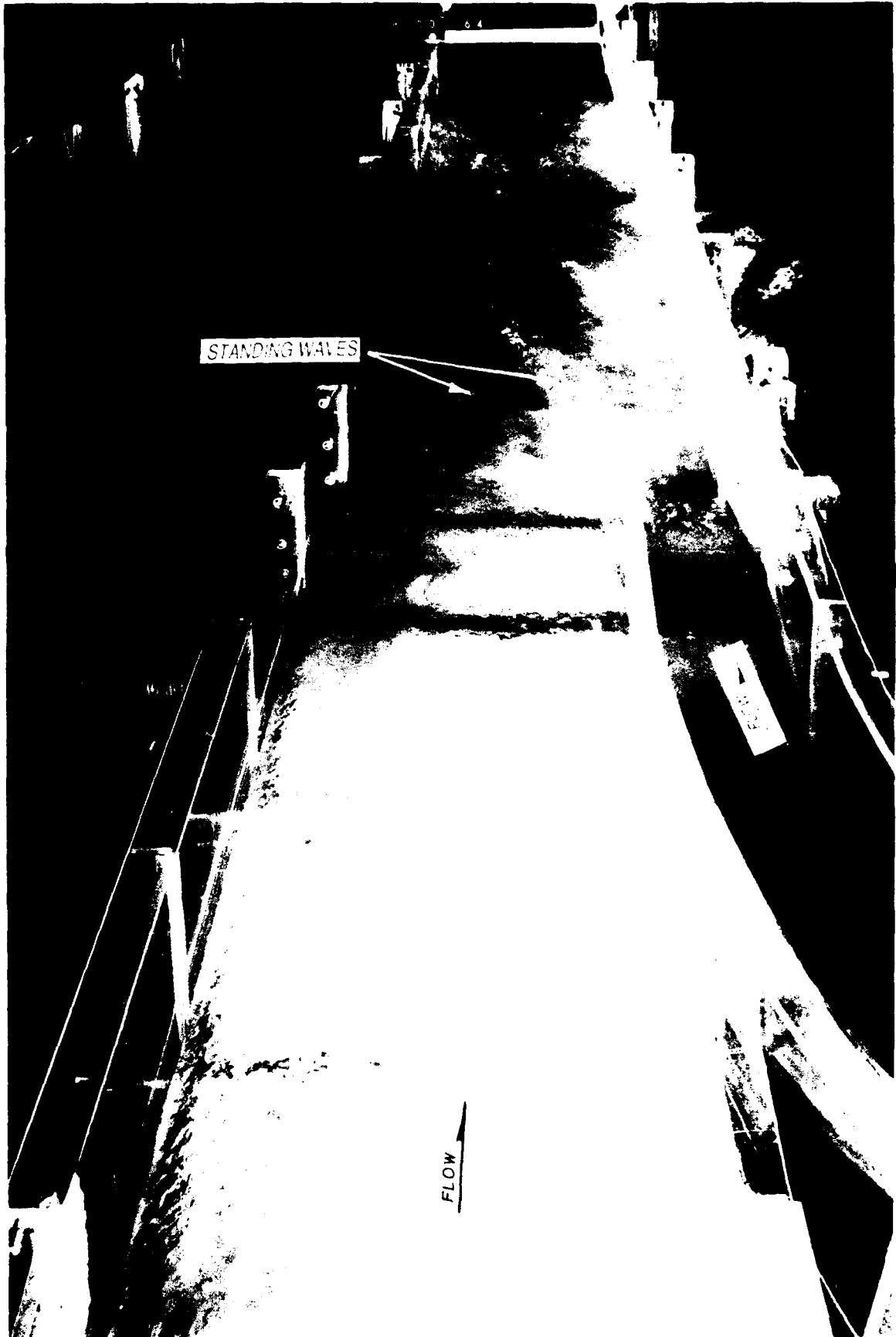


Figure 14. Flow conditions in the supercritical confluence physical model

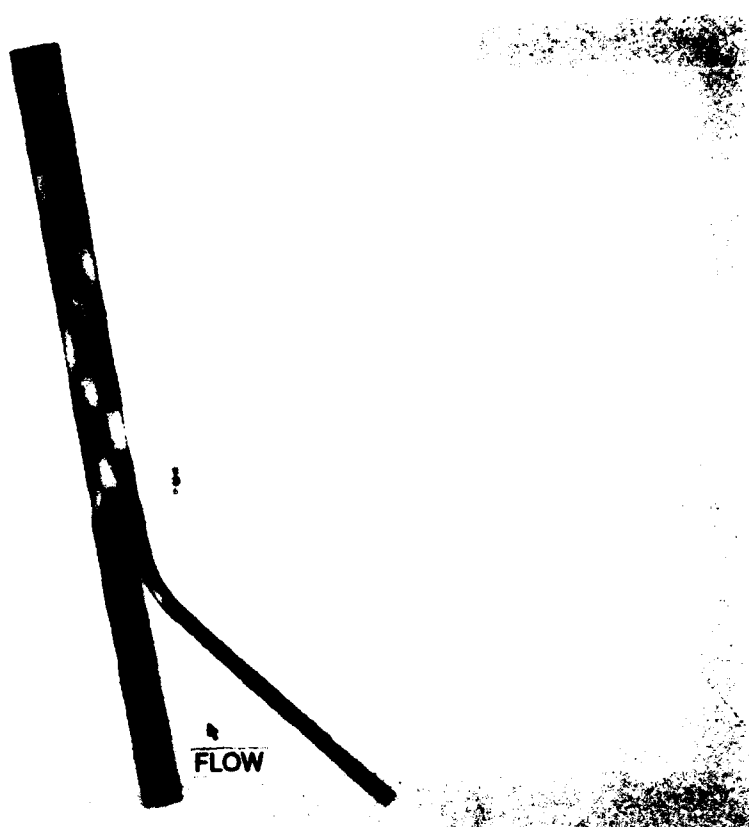


Figure 15. Depth contours in the supercritical confluence computed by HIVE2D (lighter contours indicate deeper depths)

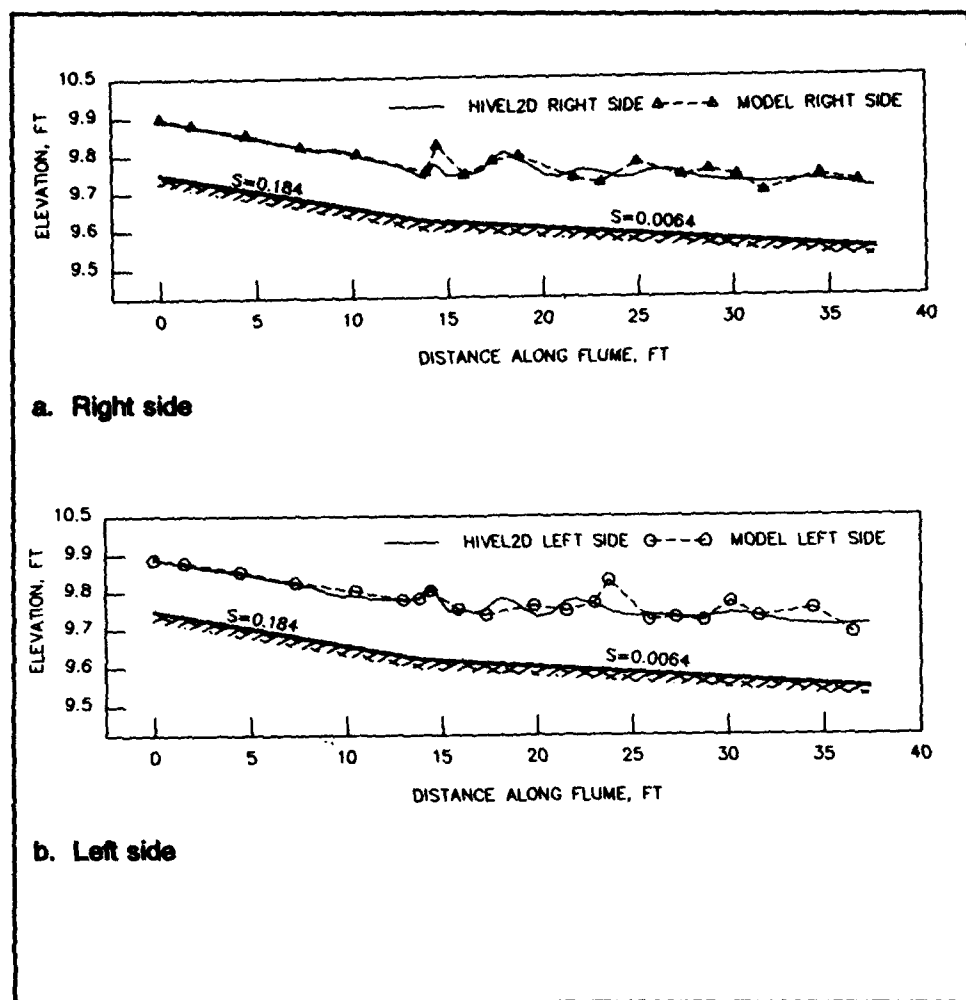


Figure 16. Water-surface profiles for the supercritical confluence problem

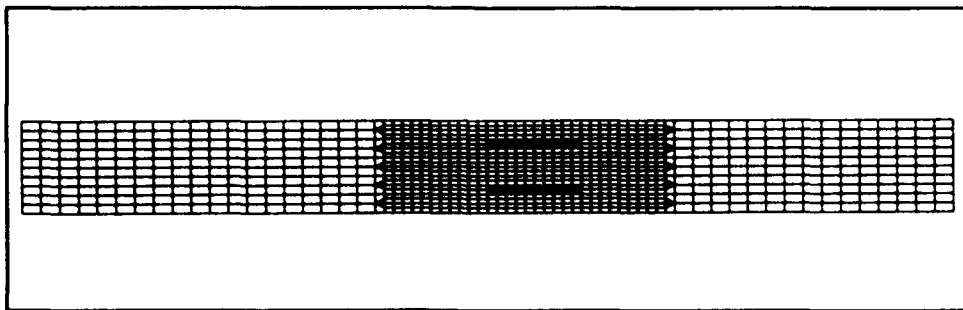


Figure 17. Numerical model computational mesh for the bridge pier problem

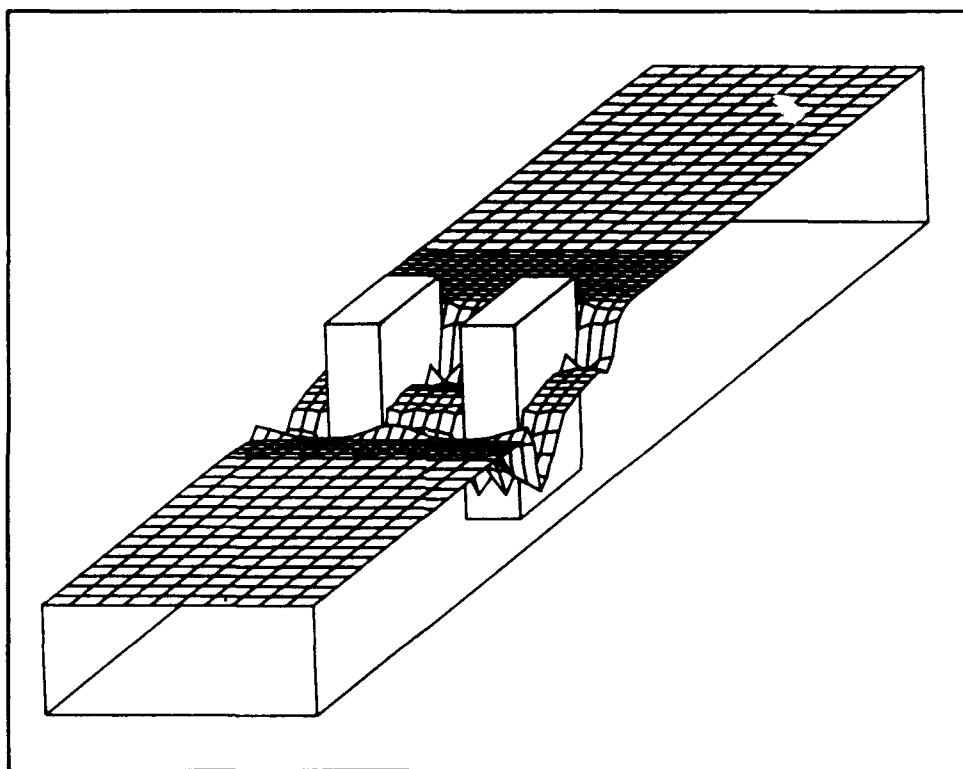


Figure 18. Oblique view of the water-surface mesh of the bridge pier problem
(flow is from upper right to lower left)

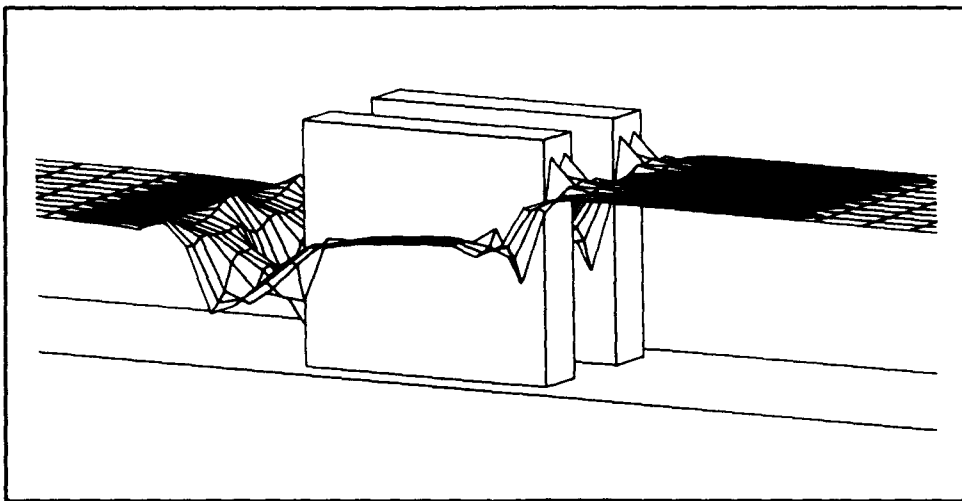


Figure 19. Side view of the water-surface mesh of the bridge pier problem
(flow is from right to left)

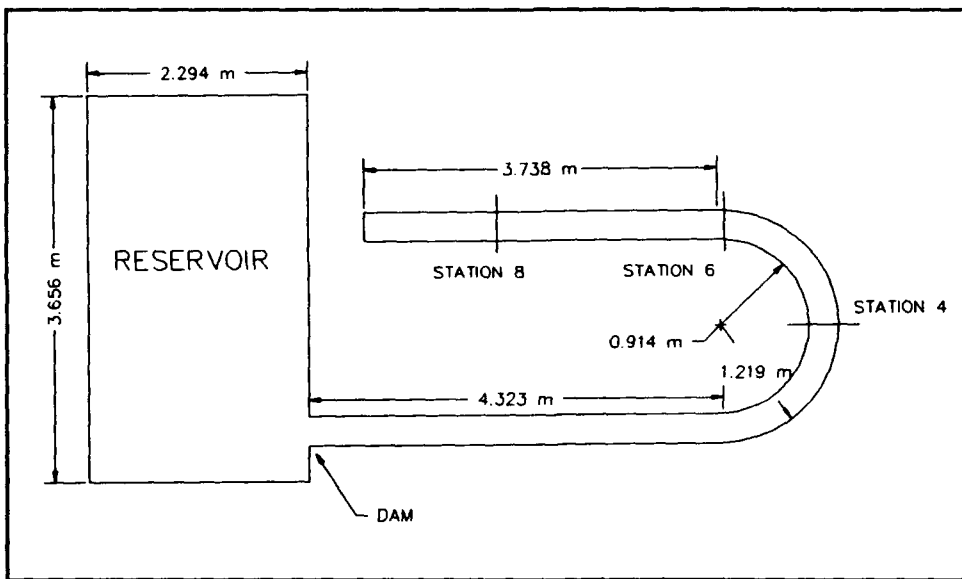


Figure 20. Details of the dam break test flume (modified from Bell, Elliot, and Chaudhry 1992)

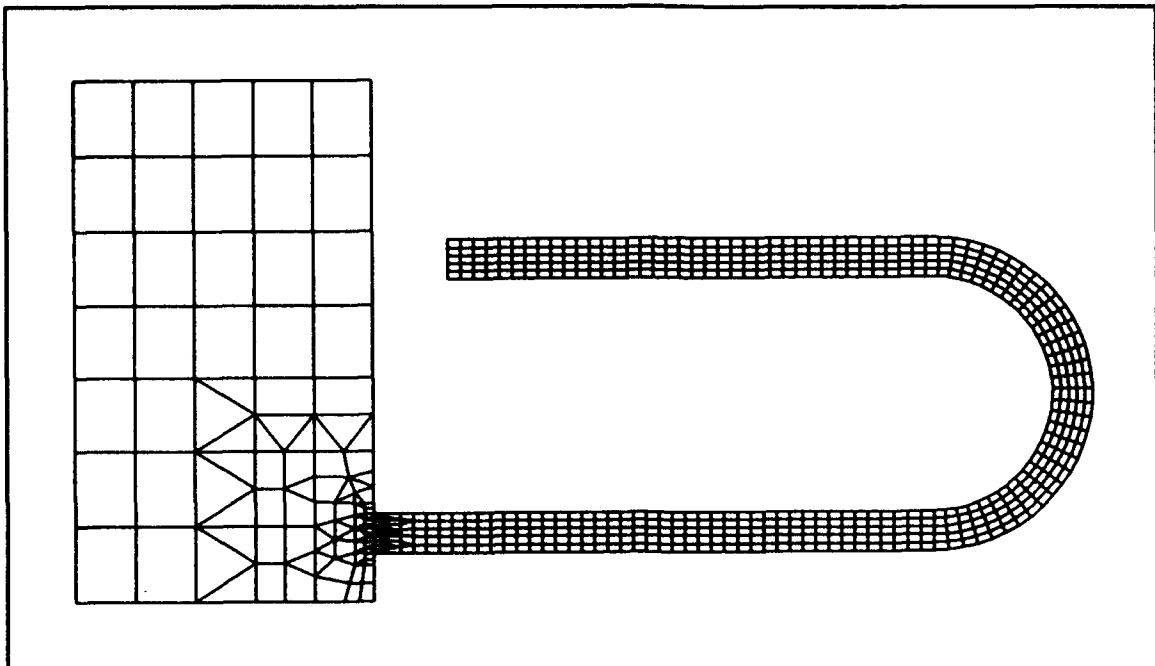


Figure 21. Numerical model computational mesh for the dam break problem

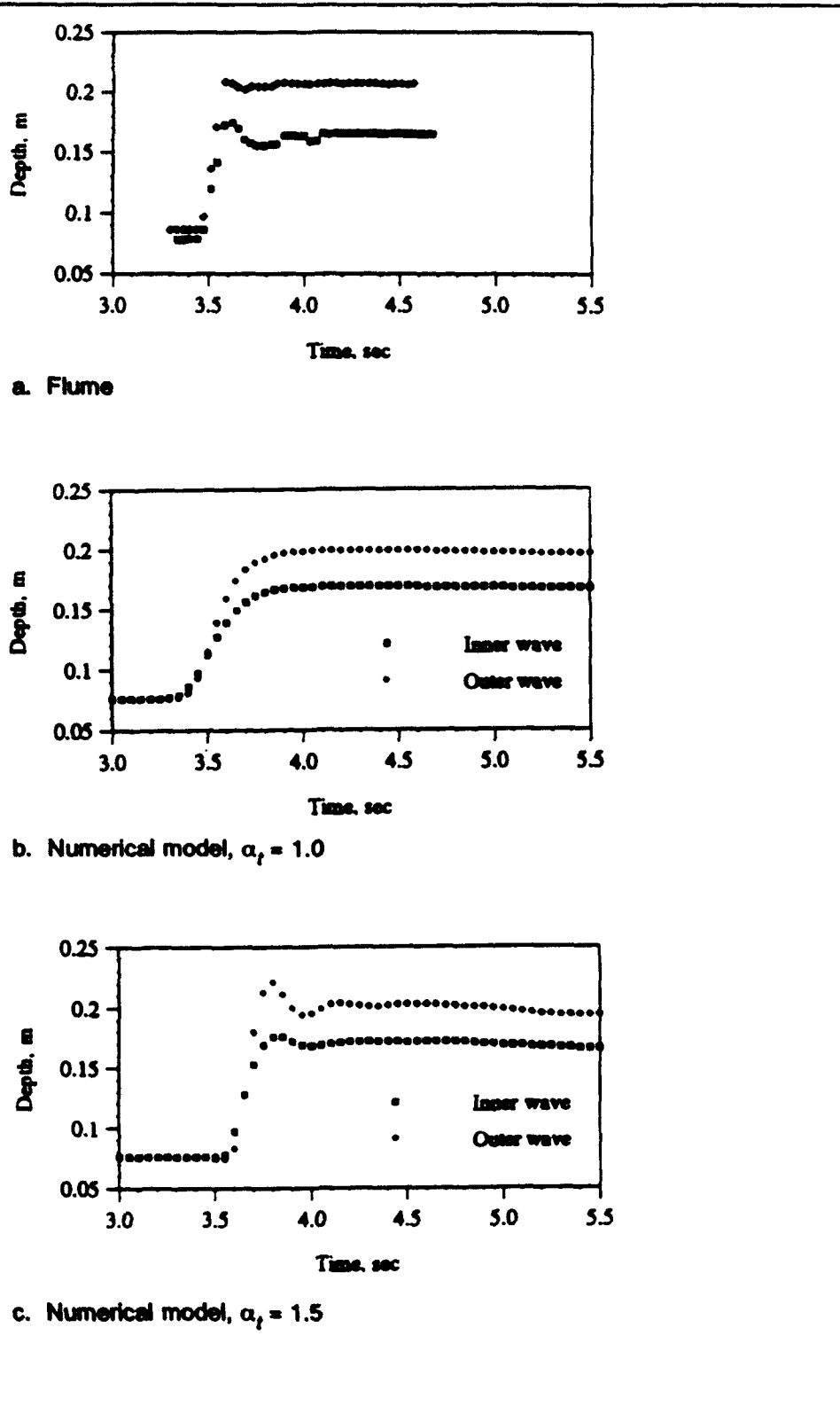
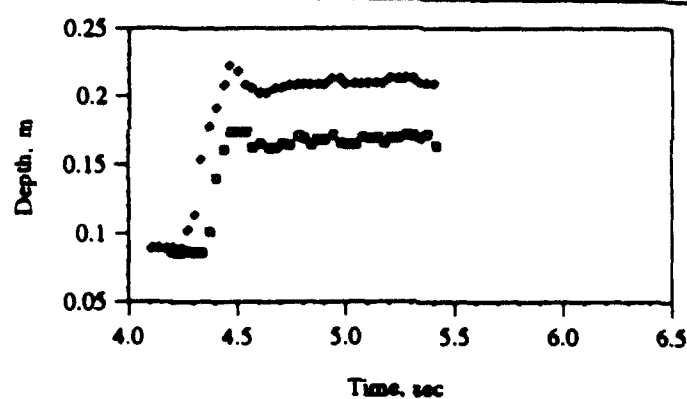
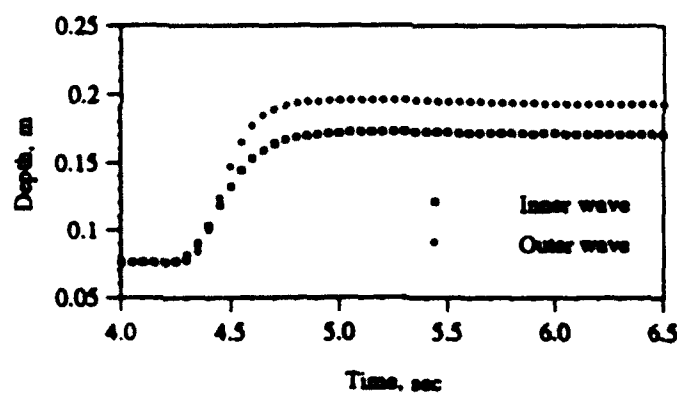


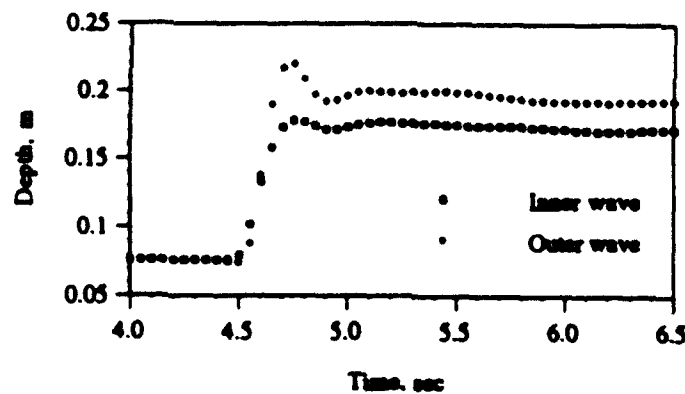
Figure 22. Flume and numerical model depth histories for station 4



a. Flume

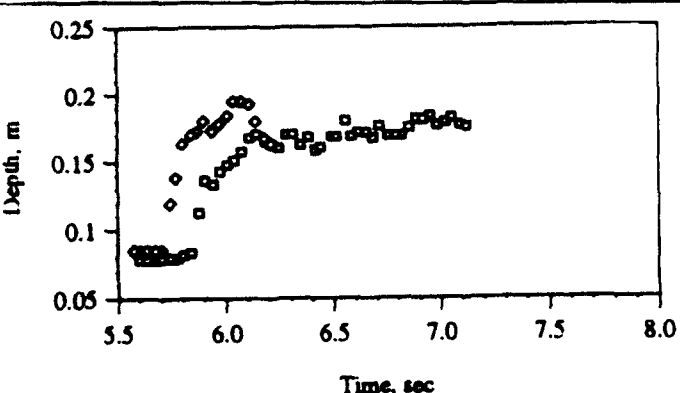


b. Numerical model, $\alpha_t = 1.0$

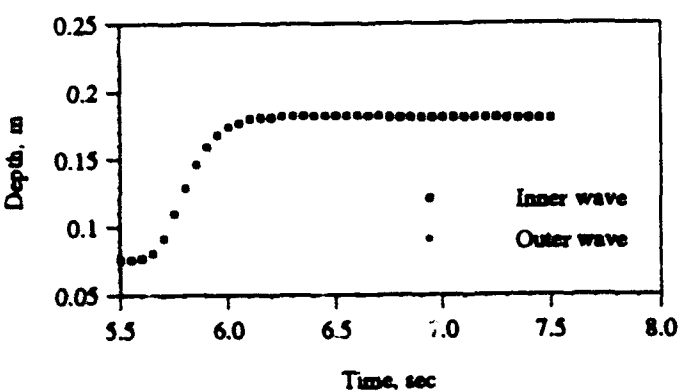


c. Numerical model, $\alpha_t = 1.5$

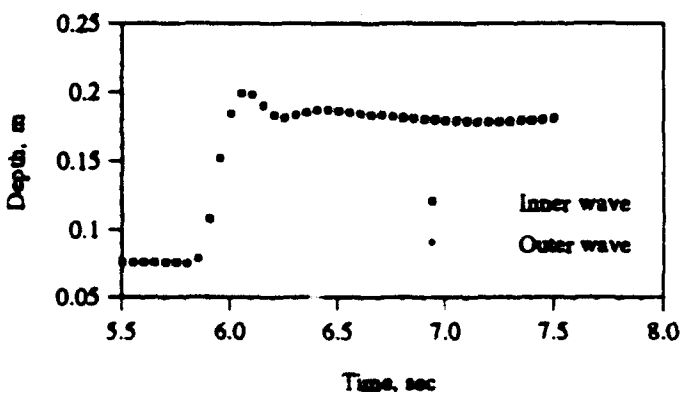
Figure 23. Flume and numerical model depth histories for station 6



a. Flume



b. Numerical model, $\alpha_i = 1.0$



c. Numerical model, $\alpha_i = 1.5$

Figure 24. Flume and numerical model depth histories for station 8

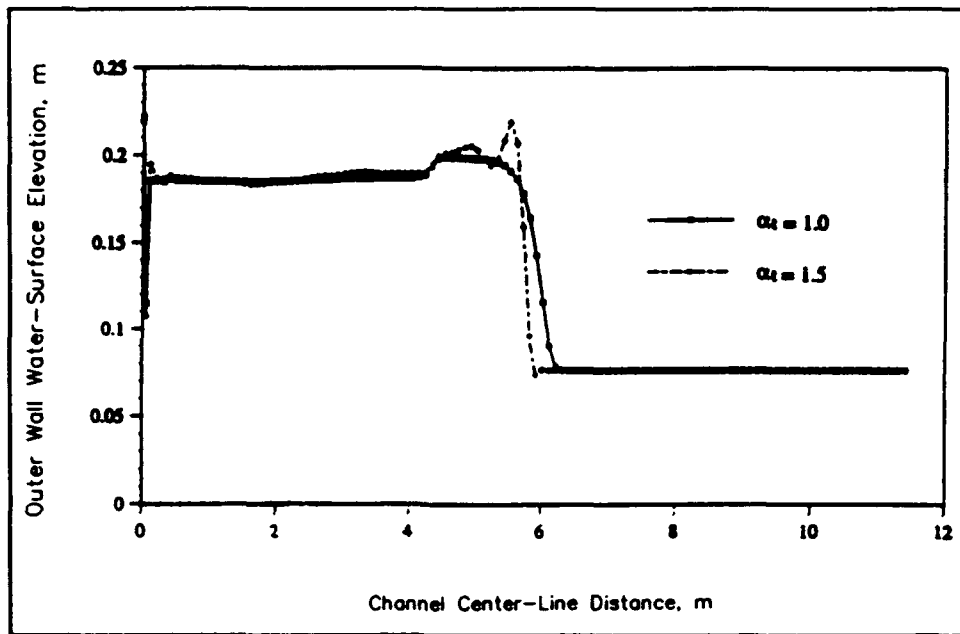


Figure 25. Water-surface elevations for dam break, comparison of temporal representation, for time of 3.5 sec

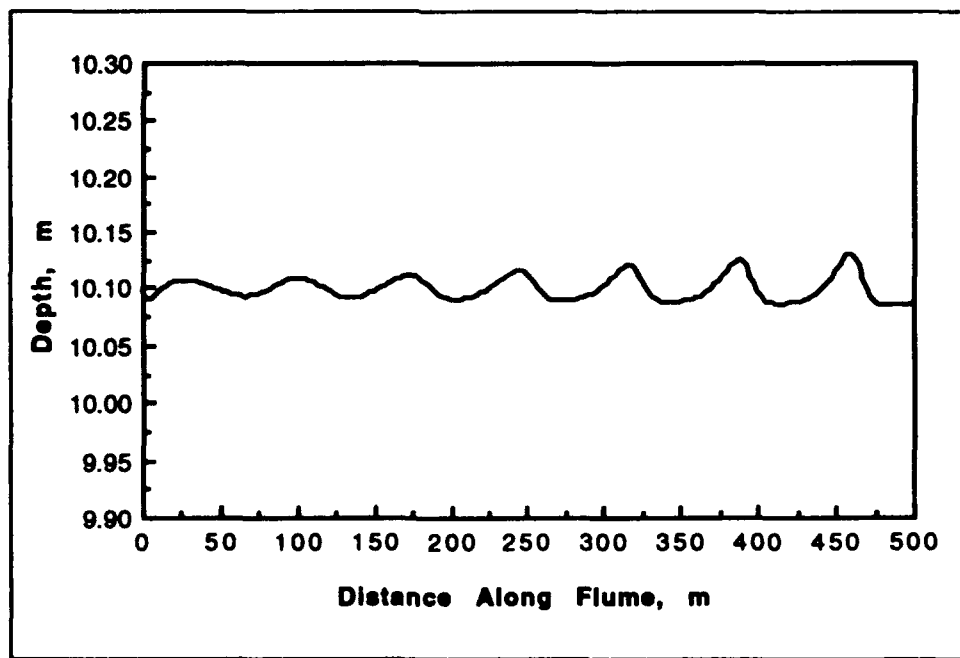


Figure 26. Depth profiles for the roll wave problem

Appendix A Governing Equations

Vertical integration of the three-dimensional equations of mass and momentum conservation for incompressible flow with the assumption that vertical velocities and accelerations are negligible compared to horizontal motions and the acceleration of gravity results in the governing equations commonly referred to as the shallow-water equations. The dependent variables of the two-dimensional fluid motion are defined by the flow depth h , the x -direction component of unit discharge p , and the y -direction component of unit discharge q . These variables are functions of the independent variables x and y , the two space directions, and time t . Neglecting free-surface stresses and the effects of Coriolis force as these are not considered important in high-velocity channels, the shallow-water equations in conservative form are given as (Abbott 1979; Praagman 1979):¹

$$\frac{\partial h}{\partial t} + \frac{\partial p}{\partial x} + \frac{\partial q}{\partial y} = 0 \quad (\text{A1})$$

for the conservation of mass. Conservation of momentum in the x -direction and y -direction are given respectively as:

$$\begin{aligned} \frac{\partial p}{\partial t} + \frac{\partial}{\partial x} \left(\frac{p^2}{h} + \frac{1}{2} gh^2 - h\sigma_{xx} \right) + \frac{\partial}{\partial y} \left(\frac{pq}{h} - h\sigma_{xy} \right) \\ = -gh \frac{\partial z}{\partial x} + g \frac{n^2 p \sqrt{p^2 + q^2}}{C_0 h^{7/3}} \end{aligned} \quad (\text{A2})$$

and

¹ References cited in this Appendix are listed in the References at the end of the main text.

$$\begin{aligned}\frac{\partial q}{\partial t} + \frac{\partial}{\partial x} \left(\frac{pq}{h} - h\sigma_{yx} \right) + \frac{\partial}{\partial y} \left(\frac{q^2}{h} + \frac{1}{2}gh^2 - h\sigma_{yy} \right) \\ = -gh \frac{\partial z}{\partial y} + g \frac{n^2 q \sqrt{p^2 + q^2}}{C_0 h^{7/3}}\end{aligned}\quad (\text{A3})$$

where

g = acceleration of gravity

$\sigma_{xx}, \sigma_{xy}, \sigma_{yx}, \sigma_{yy}$ = Reynolds stresses per unit mass where the first subscript indicates the direction and the second indicates the face on which the stress acts

z = channel invert elevation

n = Manning's roughness coefficient

C_0 = dimensional constant ($C_0 = 1$ for SI units and 2.208 for non-SI units)

The governing equations are given in vector form as:

$$\frac{\partial \mathbf{Q}}{\partial t} + \frac{\partial \mathbf{F}_x}{\partial x} + \frac{\partial \mathbf{F}_y}{\partial y} + \mathbf{H} \approx \mathbf{0} \quad (\text{A4})$$

where

$$\mathbf{Q} = \begin{bmatrix} h \\ p \\ q \end{bmatrix} \quad (\text{A5})$$

$$\mathbf{F}_x = \begin{bmatrix} p \\ \frac{p^2}{h} + \frac{1}{2}gh^2 - h\sigma_{xx} \\ \frac{pq}{h} - h\sigma_{yx} \end{bmatrix} \quad (\text{A6})$$

$$F_y = \begin{pmatrix} q \\ \frac{pq}{h} - h\sigma_{xy} \\ \frac{q^2}{h} + \frac{1}{2}gh^2 - h\sigma_{yy} \end{pmatrix} \quad (A7)$$

$$H = \begin{pmatrix} 0 \\ gh\frac{\partial z}{\partial x} - g\frac{n^2 p \sqrt{p^2 + q^2}}{C_0^2 h^{7/3}} \\ gh\frac{\partial z}{\partial y} - g\frac{n^2 q \sqrt{p^2 + q^2}}{C_0^2 h^{7/3}} \end{pmatrix} \quad (A8)$$

where

$p = uh$, u being the depth-averaged x -direction component of velocity

$q = vh$, v being the depth-averaged y -direction component of velocity

The Reynolds stresses are determined using the Boussinesq approach of gradient-diffusion:

$$\begin{aligned} \sigma_{xx} &= 2v_t \frac{\partial u}{\partial x} \\ \sigma_{xy} &= \sigma_{yx} = v_t \left(\frac{\partial u}{\partial y} + \frac{\partial v}{\partial x} \right) \\ \sigma_{yy} &= 2v_t \frac{\partial v}{\partial y} \end{aligned} \quad (A9)$$

Where v_t is the viscosity (sum of turbulent and molecular viscosity, commonly referred to as eddy viscosity), which varies spatially and is solved empirically as a function of local flow variables (Rodó 1980; Chapman and Kuo 1985):

$$v_t = C_b \sqrt{8g} \frac{n}{C_o} \frac{\sqrt{p^2 + q^2}}{h^{1/6}} \quad (A10)$$

where C_b is a coefficient that varies between 0.1 and 1.0.

This system of equations constitutes a hyperbolic initial boundary value problem. Appropriate boundary conditions are determined using the approach of Daubert and Graffe as discussed in Drolet and Gray (1988) and Verboom, Stelling, and Officier (1982). Daubert and Graffe use the method of characteristics to determine the required boundary conditions. The number of boundary conditions is equal to the number of characteristic half-planes that originate exterior to the domain and enter it. If the inflow boundary is supercritical, then all information from outside the domain is carried through this boundary. Therefore, p and q (or u and v) and the depth h must be specified. If the inflow boundary is subcritical, then the depth is influenced from the flow inside the domain (downstream control) and therefore only p and q (or u and v) are specified. Outflow boundary conditions required are determined by analysis of information transported through this boundary. If the outflow boundary is supercritical, then all information is determined within the domain and no boundary conditions are specified. However, if the outflow boundary is subcritical, then the depth of flow at the boundary (tailwater) must be specified. The no-flux boundary condition is appropriate at the sidewall boundaries and is discussed in detail in Appendix B.

Appendix B

Finite Element Formulation

A variational formulation of the governing equations involves finding a solution of the dependent variables Q using the test function Ψ over the domain Ω . The variational formulation of the shallow-water equations in integral form is:

$$\int \Psi \left(\frac{\partial Q}{\partial t} + \frac{\partial F_x}{\partial x} + \frac{\partial F_y}{\partial y} + H \right) d\Omega = 0 \quad (B1)$$

where t is time and Q , F_x , F_y , and H are defined in Equations A5-A8.

The finite element approach taken is a Petrov-Galerkin formulation that incorporates a combination of the Galerkin test function and a non-Galerkin component to control oscillations due to convection. The finite element form of the governing equations is:

$$\sum_e \left[\int_e \psi_i \left(\frac{\partial \tilde{Q}}{\partial t} + \frac{\partial \tilde{F}_x}{\partial x} + \frac{\partial \tilde{F}_y}{\partial y} + \tilde{H} \right) d\Omega_e \right] = 0, \text{ for each } i \quad (B2)$$

where

e = subscript indicating a particular element

i = subscript indicating a particular test function

\sim = discrete value of the quantity

The geometry and flow variables are represented using the Lagrange basis ϕ :

$$\bar{Q} = \sum_j \phi_j Q_j \quad (B3)$$

where j is the nodal location. Bilinear triangular and quadrilateral elements are used with nodes at the element corners. Figure B1 shows the two bilinear elements used in terms of local coordinates ξ and η .

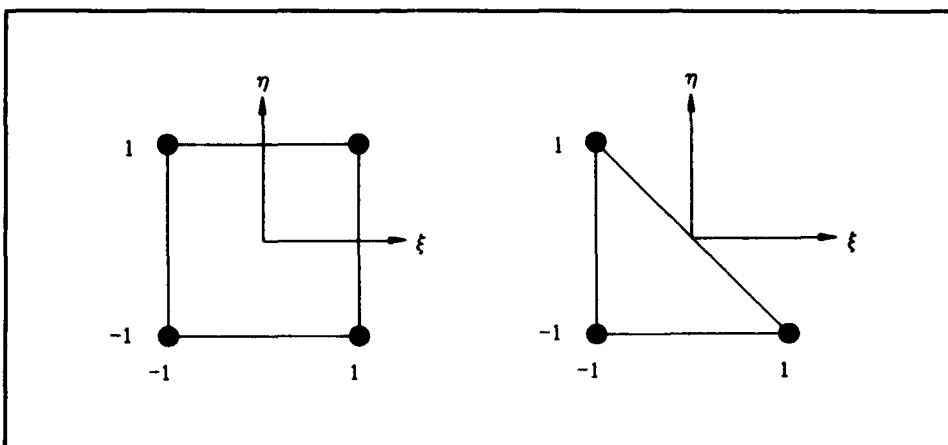


Figure B1. Local bilinear elements

The test function used (to be elaborated in the next section) is:

$$\psi_i = \phi_i I + \varphi_i \quad (B4)$$

where

ϕ_i = Galerkin part of the test function

I = identity matrix

φ_i = non-Galerkin part of the test function

To facilitate the specification of boundary conditions, the weak form of the equations is developed using an integration by parts procedure. Integration by parts of the terms

$$\phi_i \frac{\partial F_x}{\partial x}$$

$$\phi_i \frac{\partial F_y}{\partial y} \quad (B5)$$

yields the weak form of the equations. The \sim is omitted for clarity and the variables are understood to be discrete values. The weak form is given as:

$$\sum_e \left[\int_{\Omega_e} \left(\psi_i \frac{\partial Q}{\partial t} - \frac{\partial \phi_i}{\partial x} F_x - \frac{\partial \phi_i}{\partial y} F_y + \varphi_i A \frac{\partial Q}{\partial x} + \varphi_i B \frac{\partial Q}{\partial y} \right. \right. \\ \left. \left. + \psi_i H \right) d\Omega_e + \oint_{\Gamma_e} \phi_i (F_x n_x + F_y n_y) d\Gamma_e \right] = 0 \quad (B6)$$

where $(n_x, n_y) = \hat{n}$, the unit vector outward normal to the boundary Γ_e , and

$$A = \frac{\partial F_x}{\partial Q}$$

$$B = \frac{\partial F_y}{\partial Q} \quad (B7)$$

Natural boundary conditions are applied to the sidewall boundaries through the weak statement. The sidewall boundaries are "no flux" boundaries. That is, there is no net flux of mass nor momentum through these boundaries. This boundary condition is enforced in an average sense through the weak statement. Setting the mass flux through the sidewall boundary to zero:

$$\oint_{\Gamma} (pn_x + qn_y) d\Gamma = 0 \quad (B8)$$

where

p = x-direction component of unit discharge

q = y-direction component of unit discharge

There is no net momentum flux through the boundaries. Therefore, the x-direction momentum through the boundary is set to zero:

$$\oint_{\Gamma} [(up)n_x + (uq)n_y] d\Gamma = 0 \quad (B9)$$

and the y-direction momentum through the boundary is set to zero:

$$\oint_{\Gamma} [(vp)n_x + (vq)n_y] d\Gamma = 0 \quad (B10)$$

where

$u = p/h$ = the depth-averaged x-direction component of velocity

$v = q/h$ = the depth-averaged y-direction component of velocity

h = the depth of flow

Sidewall drag is treated as a partial slip condition. That is the boundary stress terms in the governing equations, integrated along the sidewall, are specified via the Manning relation:

$$-\int_{\Gamma} \phi_i (h\sigma_{xx}n_x + h\sigma_{yy}n_y) d\Gamma = \int_{\Gamma} \phi_i g p \frac{n^2 \sqrt{p^2 + q^2}}{C_0^{4/3}} d\Gamma \quad (B11)$$

and

$$-\int_{\Gamma} \phi_i (h\sigma_{yx}n_x + h\sigma_{xy}n_y) d\Gamma = \int_{\Gamma} \phi_i g q \frac{n^2 \sqrt{p^2 + q^2}}{C_0^{4/3}} d\Gamma \quad (B12)$$

where

$\sigma_{xx}, \sigma_{xy}, \sigma_{yx}, \sigma_{yy}$ = Reynolds stresses per unit mass where the first subscript indicates the direction and the second indicates the face on which the stress acts

g = acceleration of gravity

C_0 = dimensional constant ($C_0 = 1$ for SI units and 2.208 for non-SI units)

Petrov-Galerkin Test Function

For the shallow-water equations in conservative form (Equation B2), the Petrov-Galerkin test function φ_i is defined as (Berger 1993)¹:

$$\varphi_i = \beta \left[\Delta x \frac{\partial \phi_i}{\partial x} \hat{A} + \Delta y \frac{\partial \phi_i}{\partial y} \hat{B} \right] \quad (\text{B13})$$

where β is a dimensionless number between 0 and 0.5, and ϕ is the linear basis function. In the manner of Katopodes (1986) the grid intervals are chosen as:

$$\Delta x = 2 \left[\left(\frac{\partial x}{\partial \xi} \right)^2 + \left(\frac{\partial x}{\partial \eta} \right)^2 \right]^{1/2} \quad (\text{B14})$$

and

$$\Delta y = 2 \left[\left(\frac{\partial y}{\partial \xi} \right)^2 + \left(\frac{\partial y}{\partial \eta} \right)^2 \right]^{1/2} \quad (\text{B14})$$

where ξ and η are the local coordinates defined from -1 to 1 (Figure B1).

To find \hat{A} consider the following:

$$A = \frac{\partial F_x(Q)}{\partial Q} \quad (\text{B16})$$

$$P^{-1} \Lambda P = A \quad (\text{B17})$$

where $\Lambda = I\lambda$ is the matrix of eigenvalues of A , and P and P^T are made up of the right and left eigenvectors.

¹ References cited in this appendix are listed in the References at the end of the main text.

$$\hat{A} = P^{-1} \hat{\Lambda} P \quad (B18)$$

where

$$\hat{\Lambda} = \begin{bmatrix} \frac{\lambda_1}{(\lambda_1^2 + v^2)^{1/2}} & 0 & 0 \\ 0 & \frac{\lambda_2}{(\lambda_2^2 + v^2)^{1/2}} & 0 \\ 0 & 0 & \frac{\lambda_3}{(\lambda_3^2 + v^2)^{1/2}} \end{bmatrix} \quad (B19)$$

and

$$\lambda_1 = u + c \quad (B20)$$

$$\lambda_2 = u - c \quad (B21)$$

$$\lambda_3 = u \quad (B22)$$

$$c = (gh)^{1/2} \quad (B23)$$

A similar operation may be performed to define \hat{R}

This particular test function is weighted upstream along characteristics similar to a concept like that developed in the finite difference method of Courant, Isaacson, and Rees (1952) for one-sided differences. These ideas were expanded to more general problems by Moretti (1979) and Gabutti (1983) as split-coefficient matrix methods and by the generalized flux vector splitting proposed by Steger and Warming (1981). In the finite element community, instead of one-sided differences the test function is weighted upstream. This particular method in one dimension (1-D) is equivalent to the SUPG (streamline upwind Petrov-Galerkin) scheme of Hughes and Brooks (1982) and similar to the form proposed by Dendy (1974). Examples of this approach in the open channel environment using the generalized shallow-water equations are presented for 1-D in Berger and Winant (1991) and for 2-D in

Berger (1992). A 1-D St. Venant application is given by Hicks and Steffler (1992).

Shock Capturing

Berger (1993) shows that the Petrov-Galerkin scheme is not only a good scheme for advection-dominated flow, but is also a good scheme for shock capturing because the scheme dissipates energy at the short wavelengths. When a shock is encountered, the weak solution of the shallow-water equations must lose mechanical energy. Some of this energy loss is analogous to a physical hydraulic system losing energy to heat, particle rotation, etc; but much of it is, in fact, simply the energy being transferred into vertical motion. And since vertical motion is not included in the shallow-water equations, it is lost. This apparent energy loss can be advantageous.

To apply a high value of β , say 0.5, only in regions in which it is needed, since a lower value is more precise, construct a trigger mechanism that can detect shocks and increase β automatically. The method employed detects energy variation for each element and flags those elements that have a high variation as needing a larger value of β for shock capturing. Note that this would work even in a Galerkin scheme since this trigger is concerned with energy variation on an element basis and the Galerkin method would enforce energy conservation over a test function (which includes several elements).

The shock capturing is implemented when Equation B24 is true

$$Ts_i > \gamma \quad (\text{B24})$$

where γ is a specified constant and

$$Ts_i = \frac{ED_i - \bar{E}}{S} \quad (\text{B25})$$

where ED_i , the element energy deviation, is calculated by

$$ED_i = \frac{\left[\int_a^b (E - \bar{E}_i)^2 dx \right]^{1/2}}{a_i} \quad (\text{B26})$$

where

Ω_i = element i

E = mechanical energy

a_i = area of element i

and \bar{E}_i , the average energy of element i , is calculated by

$$\bar{E}_i = \frac{\int_{\Omega_i} E d\Omega}{a_i} \quad (\text{B27})$$

and

\bar{E} = the average element energy over the entire grid

S = the standard deviation of all $E D_i$

Through trial a value of γ of 1.0 was chosen.

Temporal Derivatives

A finite difference expression is used for the temporal derivatives. The general expression for the temporal derivative of a variable, Q_j , is:

$$\left[\frac{\partial Q_j}{\partial t} \right]^{m+1} \approx \alpha \left[\frac{Q_j^{m+1} - Q_j^m}{t^{m+1} - t^m} \right] + (1 - \alpha) \left[\frac{Q_j^m - Q_j^{m-1}}{t^m - t^{m-1}} \right] \quad (\text{B28})$$

where

α = temporal difference coefficient

j = nodal location

m = time-step

An α equal to 1 results in a first-order backward difference approximation and an α equal to 1.5 results in a second-order backward difference approximation of the temporal derivative.

Solution of the Nonlinear Equations

The system of nonlinear equations is solved using the Newton-Raphson iterative method (Carnahan, Luther, and Wilkes 1969). Let \mathbf{R}_i be a vector of the nonlinear equations computed using a particular test function ψ_i and using an assumed value of \mathbf{Q}_j . \mathbf{R}_i is the residual error for a particular test function i . Subsequently, \mathbf{R}_i is forced toward zero as:

$$\frac{\partial \mathbf{R}_i^k}{\partial Q_j^k} \Delta q_j^k = -\mathbf{R}_i^k \quad (B29)$$

where k is the iteration number, j is the node location, and the derivatives composing the Jacobian are determined analytically. This system of equations is solved for Δq_j^k and then an improved estimate for \mathbf{Q}_j^{k+1} is obtained from:

$$\mathbf{Q}_j^{k+1} = \mathbf{Q}_j^k + \Delta q_j^k \quad (B30)$$

This procedure is continued until convergence to an acceptable residual error is obtained.

Equation B29 represents a system of linear algebraic equations that must be solved for each iteration and each time-step. A "Profile" solver is implemented to achieve efficient coefficient matrix storage. This method stores the upper triangular portion of the coefficient matrix by columns and the lower by rows. Any zeros outside the profile are not stored or involved in the computations. The necessary arrays are then a vector composed of the columns of the upper portion and a pointer vector to locate the diagonal entries. Triangular decomposition of the coefficient matrix is used in a direct solution. The program to construct the triangular decomposition of the coefficient matrix uses a compact Crout variation of Gauss Elimination.

REPORT DOCUMENTATION PAGE

*Form Approved
OMB No. 0704-0188*

Public reporting burden for this collection of information is estimated to average 1 hour per response, including the time for reviewing instructions, searching existing data sources, gathering and maintaining the data needed, and completing and reviewing the collection of information. Send comments regarding this burden estimate or any other aspect of this collection of information, including suggestions for reducing this burden, to Washington Headquarters Services, Directorate for Information Operations and Reports, 1215 Jefferson Davis Highway, Suite 1204, Arlington, VA 22202-4302, and to the Office of Management and Budget, Paperwork Reduction Project (0704-0188), Washington, DC 20503.

1. AGENCY USE ONLY (Leave blank)			2. REPORT DATE November 1994		3. REPORT TYPE AND DATES COVERED Final report	
4. TITLE AND SUBTITLE HIVEL2D: A Two-Dimensional Flow Model for High-Velocity Channels			5. FUNDING NUMBERS WU 32657			
6. AUTHOR(S) R. L. Stockstill R. C. Berger						
7. PERFORMING ORGANIZATION NAME(S) AND ADDRESS(ES) U.S. Army Engineer Waterways Experiment Station 3909 Halls Ferry Road, Vicksburg, MS 39180-6199			8. PERFORMING ORGANIZATION REPORT NUMBER Technical Report REMR-HY-12			
9. SPONSORING/MONITORING AGENCY NAME(S) AND ADDRESS(ES) U.S. Army Corps of Engineers, Washington, DC 20314-1000			10. SPONSORING/MONITORING AGENCY REPORT NUMBER 			
11. SUPPLEMENTARY NOTES Available from National Technical Information Service, 5285 Port Royal Road, Springfield, VA 22161.						
12a. DISTRIBUTION/AVAILABILITY STATEMENT Approved for public release; distribution is unlimited.				12b. DISTRIBUTION CODE		
13. ABSTRACT (Maximum 200 words) A numerical flow model, HIVEL2D, has been developed as a tool to evaluate high-velocity channels. HIVEL2D is a depth-averaged, two-dimensional flow model designed specifically for flow fields that contain supercritical and subcritical regimes as well as the transitions between the regimes. The model is a finite element description of the two-dimensional shallow-water equations in conservative form. Provided in this report are a description of the numerical flow model and illustrative examples of typical high-velocity flow fields that the model is capable of simulating. Model verification is obtained by comparison of simulation results with data obtained from flume studies. Model assumptions and limitations are also discussed.						
14. SUBJECT TERMS Finite element method High-velocity channels Hydraulic jump (strong shock)				15. NUMBER OF PAGES 53		
16. PRICE CODE						
17. SECURITY CLASSIFICATION OF REPORT UNCLASSIFIED	18. SECURITY CLASSIFICATION OF THIS PAGE UNCLASSIFIED	19. SECURITY CLASSIFICATION OF ABSTRACT	20. LIMITATION OF ABSTRACT			